Figure 4 Morphological analysis of cranial motor nuclei. (A–E) Immunofluorescent analysis (TDP-43, green; ChAT, red) of motor neurons in the trigeminal motor (m.) (A), facial (B), hypoglossal (C), oculomotor (D), and abductor (E) nuclei from 100-week-old control (n = 3) and TDP CKO mice (n = 3). Graphs show the average size and number of motor neurons in each area. TDP + = TDP-43-positive neuron; TDP − = TDP-43-negative neuron. Error bars indicate SD. Scale bars = 50 μm. MN = motor neuron; N.S. = not significant.

role of TDP-43 in postnatal mammalian neurons has not been fully elucidated. In the present study, we clarified that TDP CKO mice, in which TDP-43 was specifically knocked-out by Cre recombinase in postnatal motor neurons, develops a progressive motor neuronal degeneration as seen in ALS, suggesting that TDP-43 is essential for the long term maintenance of postnatal motor neurons in mice. Although TDP CKO mice developed ALS-like motor impairment, the mortality of the mice was not different from that of control littermates. This might be due to the knockout efficiency of TDP-43, which occurred in ∼50% of motor neurons, or due to the life span of mice, which is considerably shorter than the disease duration of patients with ALS. Moreover, there were no

significant alterations in body weight, motor function or morphology of motor neurons in our TDP heterozygous CKO (TDP hCKO) mice. Because previous studies demonstrated that the protein expression of TDP-43 was not reduced in various tissues of heterozygous TDP-43 knockout mice (Kraemer et al., 2010; Sephton et al., 2010; Wu et al., 2010), TDP-43 depletion is likely insufficient to affect the motor neurons in our TDP hCKO mice. At the same time, these data suggest that expression of Cre itself did not affect the vulnerability of the mouse motor neurons over 2 years.

An earlier study demonstrates that the motor neuron-specific TDP-43 knockout mouse carrying HB9-Cre exhibits early-onset
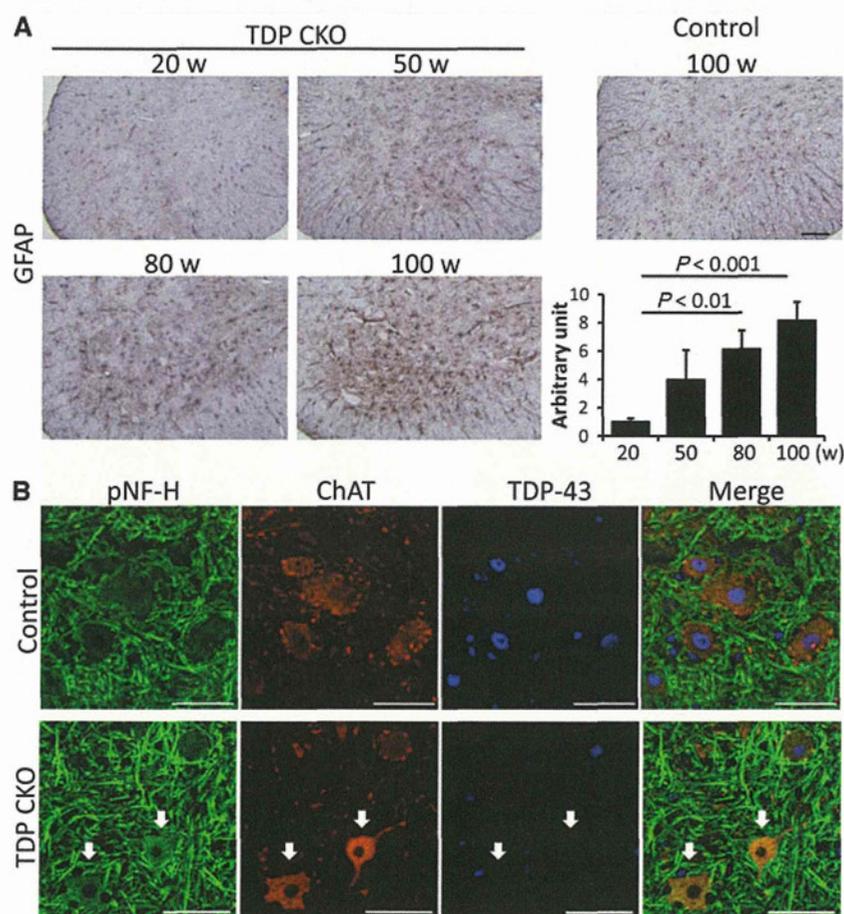
**Figure 5** Astrogliosis and neuronal accumulation of phosphorylated neurofilament. (**A**) Immunohistochemistry against GFAP in the ventral horn and a time course analysis of astrogliosis. Error bars indicate SD (*n* = 3 for each age). (**B**) Immunofluorescent staining against pNF-H (green), ChAT (red) and TDP-43 (blue). pNF-H was accumulated in the cell bodies of TDP-43-lacking motor neurons of TDP CKO mice (arrows). Scale bars: **A** = 100 μm; **B** = 50 μm.

motor dysfunction and develops motor neuronal loss earlier than 10 weeks of age (Wu *et al.*, 2012). However, given that the Cre-mediated recombination using the *HB9* promoter began at the developmental stage E9.5 (Arber *et al.*, 1999), this model possibly reflects the loss-of-function of TDP-43 in the motor neuron development. By contrast, because the Cre expression in VAChT-Cre.Fast mice is mediated by the VAChT promoter, the number of Cre-expressing motor neurons in VAChT-Cre.Fast mice is scarcely detected at prenatal stages, but becomes maximum in number at 5 weeks (Misawa *et al.*, 2003). We also confirmed that TDP-43 was not excised in spinal motor neurons of TDP CKO mice at post-natal Day 2, but knocked-out in ~50 % of motor neurons of the 10-week-old mice. This temporal pattern of Cre expression appears to contribute to the late-onset progressive motor dysfunction in our TDP CKO mice and enable the assessment of loss of TDP-43 functions in mouse motor neurons at the postnatal stage. As far as we investigated, TDP-43 was knocked-out in spinal motor neurons beginning at 10 weeks, but the function and morphology of motor neurons were unexpectedly preserved for 1 year in TDP CKO mice, suggesting that the loss of TDP-43 was compensated in motor neurons of young

mice, but triggered neuronal vulnerability with the ageing process. Given that ALS is an age-related neurodegenerative disease and that the disease develops after middle age even in inherited cases with TDP-43 mutations (Gitcho *et al.*, 2008; Kabashi *et al.*, 2008; Sreedharan *et al.*, 2008; Yokoseki *et al.*, 2008), our TDP CKO mice appear to be a model that recapitulates the age-dependent phenotypes of ALS. However, as TDP CKO mice lack some aspects of human ALS pathology, such as cytoplasmic inclusions of TDP-43 and the involvement of upper motor neurons, the use of this model for therapeutic research needs further validation.

In the histopathological analyses, TDP CKO mice exhibited the atrophy of motor neurons, degeneration of large motor axons, denervation of neuromuscular junctions and grouped atrophy of skeletal muscles, all of which are common to the pathology of human motor neuron disease. The disruption of retrograde labelling in TDP-43-lacking motor neurons suggests that TDP-43 depletion directly induces neuronal dysfunction. Interestingly, the axonal degenerations were evident in the ventral root of TDP CKO mice at 50 weeks of age, when the morphology of lumbar motor neurons was not altered. These findings are compatible with the fact that ALS pathology initially manifests at the axon
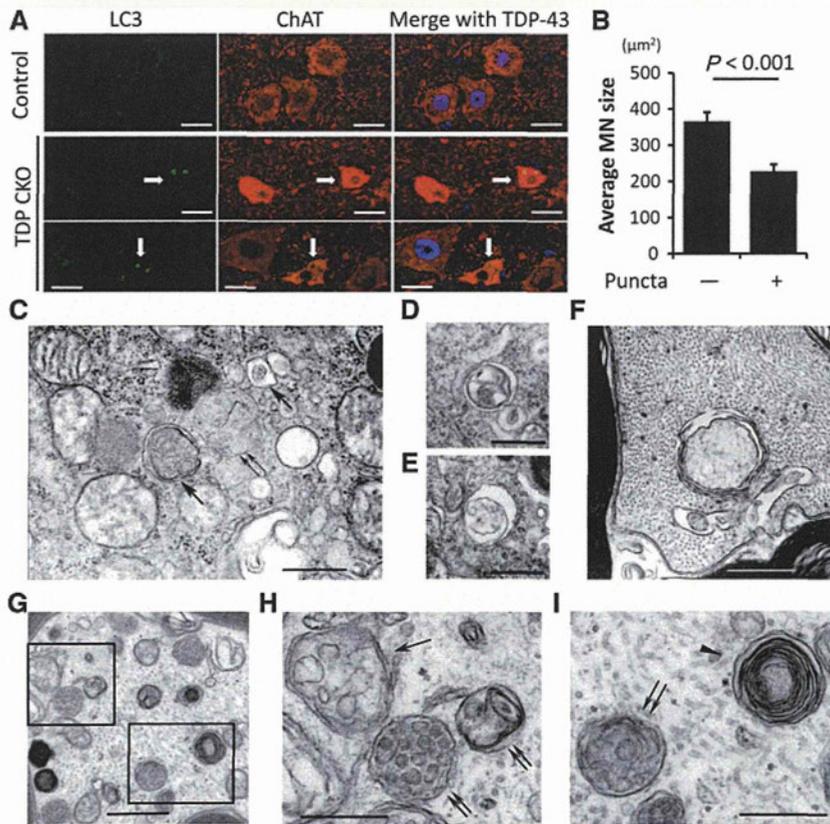
**Figure 6** Formation of autophagosomes in motor neurons of TDP CKO mice. (**A**) Immunofluorescent analysis (LC3, green; ChAT, red; TDP-43, blue) revealed LC3-positive cytoplasmic puncta in TDP-43-lacking motor neurons of 100-week-old TDP CKO mice. (**B**) The average size of TDP-43 lacking motor neurons (MN) with ($n = 25$) and without ($n = 48$) LC3-positive puncta. Error bars indicate SEM. (**C–I**) Ultrastructural analysis of 100-week-old TDP CKO mice. Autophagosomes (arrows) and an autolysosome (double arrows) (**C**), autolysosomes surrounded by a single membrane containing mitochondria (**D**) and autophagosomes containing ribosome-like structures (**E**) were observed in the cell bodies of the motor neurons. An autophagic structure in the proximal motor axon (**F**). Accumulation of organelles containing mitochondria, autophagosomes (arrows), autolysosomes (double arrows), and autophagic structure with a multi-lamelleted structure (arrowhead) in the sciatic nerve (**G**) and its enlarged images (**D, E, H and I**). Scale bars: **A** = 20 µm; **C** and **G** = 1 µm; **F, H and I** = 500 nm.

(Fischer *et al.*, 2004). The increase of small myelinated fibres accompanied by the decrease of large myelinated fibres in the ventral root of 100-week-old TDP CKO mice corresponds to the morphological change in the cell body of the motor neurons, and similar observations were also reported in the patients and mouse models of ALS (Bradley *et al.*, 1983; Zhang *et al.*, 1997). TDP CKO mice also exhibited several features that are shared with patients with sporadic ALS: the involvement in the cranial motor nuclei such as the hypoglossal nucleus, preserved morphology in the extraocular motor neurons, accumulations of phosphorylated neurofilament in motor neurons and astrogliosis in the spinal ventral horn. Dysphagia due to the involvement of the hypoglossal nucleus might enhance the weight loss in aged TDP CKO mice through decreased oral intake. In ALS, extraocular motor neurons are resistant to degeneration compared with other somatomotor neurons, and differences in calcium buffering capacities have been proposed as a possible reason for this selective vulnerability (Alexianu *et al.*, 1994; Reiner *et al.*, 1995; Laslo *et al.*, 2000). Because RNA-seq analysis demonstrates that depletion of

TDP-43 affects the calcium signalling pathway in mouse striatum (Polymenidou *et al.*, 2011), it is possible that dysregulation of calcium buffering underlies the pathogenesis of TDP CKO mice.

Our immunofluorescent analysis also demonstrated LC3-positive cytoplasmic puncta in TDP-43-depleted motor neurons, and the presence of these puncta was associated with shrinkage of motor neurons. This finding was confirmed by electron microscopy that revealed the presence of autolysosomes and autophagosomes in the motor neuronal cell bodies and axons of TDP CKO mice, suggesting that TDP-43 depletion resulted in dysregulation of the autophagic pathway. In addition, the accumulation of autophagic structures in the sciatic nerve and the disruption of retrograde labelling in TDP-43-lacking motor neurons suggest that the disruption of retrograde axonal transport may underlie the motor neuronal dysfunction in TDP CKO mice. Although the disruption of constitutive autophagy is shown to instigate the degeneration of certain types of neurons (Komatsu *et al.*, 2006), the causative role of the autophagic dysregulation in the pathogenesis of motor neuron diseases remains controversial. A recent work

demonstrates that motor neuron-specific knockout of the proteasome subunit Rpt3, but not autophagy mediator Atg7, leads to motor neuron degeneration in mice (Tashiro et al., 2012), suggesting that the disruption of autophagic pathway in motor neurons may not be the primary cause of the neurodegeneration. However, accumulation of autophagosomes and autolysosomes was observed in the motor neurons of mice with mutant SOD1 (Li et al., 2008; Tian et al., 2011) and patients with sporadic ALS (Nakano et al., 1993; Sasaki, 2011). In addition, mice carrying mutations of dynein or dynactin exhibit motor dysfunction with accumulation of autophagosomes in the motor neurons (Ravikumar et al., 2005; Laird et al., 2008). These lines of evidence may suggest a possible link between the increased autophagosomes and the process of motor neuron degeneration (Pasquali et al., 2009; Chen et al., 2012), although it remains unclear whether the accumulation of autophagosomes in neurodegenerative diseases results from activation of autophagy, disruption of retrograde transport or decreased lysosome fusion (Shintani and Klionsky, 2004; Baehrecke, 2005; Perlson et al., 2010). Further investigation with regard to the linkage among loss of TDP-43, retrograde axonal transport and dysregulation of autophagy might contribute to our understanding the pathogenesis of ALS.

In conclusion, TDP CKO mice exhibited age-dependent motor impairment and morphological alterations in the motor neuron system that recapitulate several features of sporadic ALS neuropathology, including the accumulation of autophagosomes. These findings suggest that TDP-43 plays an essential role in the long-term maintenance of motor neurons, and that loss of TDP-43 function contributes to the pathogenesis of ALS.

# Funding

# Supplementary material

Supplementary material is available at Brain online.

# References

Alexianu ME, Ho BK, Mohamed AH, La Bella V, Smith RG, Appel SH. The role of calcium-binding proteins in selective motoneuron vulnerability in amyotrophic lateral sclerosis. Ann Neurol 1994; 36: 846–58.

Arai T, Hasegawa M, Akiyama H, Ikeda K, Nonaka T, Mori H, et al. TDP-43 is a component of ubiquitin-positive tau-negative inclusions in frontotemporal lobar degeneration and amyotrophic lateral sclerosis. Biochem Biophys Res Commun 2006; 351: 602–11.

Arber S, Han B, Mendelsohn M, Smith M, Jessell TM, Sockanathan S. Requirement for the homeobox gene Hb9 in the consolidation of motor neuron identity. Neuron 1999; 23: 659–74.

Ayala YM, Misteli T, Baralle FE. TDP-43 regulates retinoblastoma protein phosphorylation through the repression of cyclin-dependent kinase 6 expression. Proc Natl Acad Sci USA 2008; 105: 3785–9.

Ayala YM, Pantano S, D'Ambrogio A, Buratti E, Brindisi A, Marchetti C, et al. Human, Drosophila, and C.elegans TDP43: nucleic acid binding properties and splicing regulatory function. J Mol Biol 2005; 348: 575–88.

Baehrecke EH. Autophagy: dual roles in life and death? Nat Rev Mol Cell Biol 2005; 6: 505–10.

Bradley WG, Good P, Rasool CG, Adelman LS. Morphometric and biochemical studies of peripheral nerves in amyotrophic lateral sclerosis. Ann Neurol 1983; 14: 267–77.

Buratti E, Brindisi A, Giombi M, Tisminetzky S, Ayala YM, Baralle FE. TDP-43 binds heterogeneous nuclear ribonucleoprotein A/B through its C-terminal tail: an important region for the inhibition of cystic fibrosis transmembrane conductance regulator exon 9 splicing. J Biol Chem 2005; 280: 37572–84.

Buratti E, De Conti L, Stuani C, Romano M, Baralle M, Baralle F. Nuclear factor TDP-43 can affect selected microRNA levels. FEBS J 2010; 277: 2268–81.

Chen S, Zhang X, Song L, Le W. Autophagy dysregulation in amyotrophic lateral sclerosis. Brain Pathol 2012; 22: 110–6.

Chiang PM, Ling J, Jeong YH, Price DL, Aja SM, Wong PC. Deletion of TDP-43 down-regulates Tbc1d1, a gene linked to obesity, and alters body fat metabolism. Proc Natl Acad Sci USA 2010; 107: 16320–4.

Feiguin F, Godena VK, Romano G, D'Ambrogio A, Klima R, Baralle FE. Depletion of TDP-43 affects Drosophila motoneurons terminal synapsis and locomotive behavior. FEBS Lett 2009; 583: 1586–92.

Fischer LR, Culver DG, Tennant P, Davis AA, Wang M, Castellano-Sanchez A, et al. Amyotrophic lateral sclerosis is a distal axonopathy: evidence in mice and man. Exp Neurol 2004; 185: 232–40.

Gitcho MA, Baloh RH, Chakraverty S, Mayo K, Norton JB, Levitch D, et al. TDP-43 A315T mutation in familial motor neuron disease. Ann Neurol 2008; 63: 535–8.

Igaz LM, Kwong LK, Lee EB, Chen-Plotkin A, Swanson E, Unger T, et al. Dysregulation of the ALS-associated gene TDP-43 leads to neuronal death and degeneration in mice. J Clin Invest 2011; 121: 726–38.

Iguchi Y, Katsuno M, Niwa J, Yamada S, Sone J, Waza M, et al. TDP-43 depletion induces neuronal cell damage through dysregulation of Rho family GTPases. J Biol Chem 2009; 284: 22059–66.

Kabashi E, Lin L, Tradewell ML, Dion PA, Bercier V, Bourgouin P, et al. Gain and loss of function of ALS-related mutations of TARDBP (TDP-43) cause motor deficits in vivo. Hum Mol Genet 2011; 19: 671–83.

Kabashi E, Valdmanis PN, Dion P, Spiegelman D, McConkey BJ, Vande Velde C, et al. TARDBP mutations in individuals with sporadic and familial amyotrophic lateral sclerosis. Nat Genet 2008; 40: 572–4.

Katsuno M, Adachi H, Kume A, Li M, Nakagomi Y, Niwa H, et al. Testosterone reduction prevents phenotypic expression in a transgenic mouse model of spinal and bulbar muscular atrophy. Neuron 2002; 35: 843–54.

Katsuno M, Adachi H, Minamiyama M, Waza M, Tokui K, Banno H, et al. Reversible disruption of dynactin 1-mediated retrograde axonal transport in polyglutamine-induced motor neuron degeneration. J Neurosci 2006; 26: 12106–17.

Komatsu M, Waguri S, Chiba T, Murata S, Iwata J, Tanida I, et al. Loss of autophagy in the central nervous system causes neurodegeneration in mice. Nature 2006; 441: 880–4.

Kraemer BC, Schuck T, Wheeler JM, Robinson LC, Trojanowski JQ, Lee VM, et al. Loss of murine TDP-43 disrupts motor function and plays an essential role in embryogenesis. Acta Neuropathol 2010; 119: 409–19.

Laird FM, Farah MH, Ackerley S, Hoke A, Maragakis N, Rothstein JD, et al. Motor neuron disease occurring in a mutant dynactin mouse

model is characterized by defects in vesicular trafficking. J Neurosci 2008; 28: 1997–2005.

Laslo P, Lipski J, Nicholson LF, Miles GB, Funk GD. Calcium binding proteins in motoneurons at low and high risk for degeneration in ALS. Neuroreport 2000; 11: 3305–8.

Lee EB, Lee VM, Trojanowski JQ. Gains or losses: molecular mechanisms of TDP43-mediated neurodegeneration. Nat Rev Neurosci 2011; 13: 38–50.

Li L, Zhang X, Le W. Altered macroautophagy in the spinal cord of SOD1 mutant mice. Autophagy 2008; 4: 290–3.

Misawa H, Nakata K, Toda K, Matsuura J, Oda Y, Inoue H, et al. VAChT-Cre. Fast and VAChT-Cre.Slow: postnatal expression of Cre recombinase in somatomotor neurons with different onset. Genesis 2003; 37: 44–50.

Nakano I, Shibata T, Uesaka Y. On the possibility of autolysosomal processing of skein-like inclusions. Electron microscopic observation in a case of amyotrophic lateral sclerosis. J Neurol Sci 1993; 120: 54–9.

Neumann M, Sampathu DM, Kwong LK, Truax AC, Micsenyi MC, Chou TT, et al. Ubiquitinated TDP-43 in frontotemporal lobar degeneration and amyotrophic lateral sclerosis. Science 2006; 314: 130–3.

Pasquali L, Longone P, Isidoro C, Ruggieri S, Paparelli A, Fornai F. Autophagy, lithium, and amyotrophic lateral sclerosis. Muscle Nerve 2009; 40: 173–94.

Perlson E, Maday S, Fu MM, Moughamian AJ, Holzbaur EL. Retrograde axonal transport: pathways to cell death? Trends Neurosci 2010; 33: 335–44.

Polymenidou M, Lagier-Tourenne C, Hutt KR, Huelga SC, Moran J, Liang TY, et al. Long pre-mRNA depletion and RNA missplicing contribute to neuronal vulnerability from loss of TDP-43. Nat Neurosci 2011; 14: 459–68.

Ravikumar B, Acevedo-Arozena A, Imarisio S, Berger Z, Vacher C, O'Kane CJ, et al. Dynein mutations impair autophagic clearance of aggregate-prone proteins. Nat Genet 2005; 37: 771–6.

Reiner A, Medina L, Figueredo-Cardenas G, Anfinson S. Brainstem motoneuron pools that are selectively resistant in amyotrophic lateral sclerosis are preferentially enriched in parvalbumin: evidence from monkey brainstem for a calcium-mediated mechanism in sporadic ALS. Exp Neurol 1995; 131: 239–50.

Sasaki S. Autophagy in spinal cord motor neurons in sporadic amyotrophic lateral sclerosis. J Neuropathol Exp Neurol 2011; 70: 349–59.

Sephton CF, Cenik C, Kucukural A, Dammer EB, Cenik B, Han Y, et al. Identification of neuronal RNA targets of TDP-43-containing ribonucleoprotein complexes. J Biol Chem 2011; 286: 1204–15.

Sephton CF, Good SK, Atkin S, Dewey CM, Mayer P III, Herz J, et al. TDP-43 is a developmentally regulated protein essential for early embryonic development. J Biol Chem 2010; 285: 6826–34.

Shan X, Chiang PM, Price DL, Wong PC. Altered distributions of Gemini of coiled bodies and mitochondria in motor neurons of TDP-43 transgenic mice. Proc Natl Acad Sci USA 2010; 107: 16325–30.

Shintani T, Klionsky DJ. Autophagy in health and disease: a double-edged sword. Science 2004; 306: 990–5.

Sreedharan J, Blair IP, Tripathi VB, Hu X, Vance C, Rogelj B, et al. TDP-43 mutations in familial and sporadic amyotrophic lateral sclerosis. Science 2008; 319: 1668–72.

Stallings NR, Puttaparthi K, Luther CM, Burns DK, Elliott JL. Progressive motor weakness in transgenic mice expressing human TDP-43. Neurobiol Dis 2010; 40: 404–14.

Strong MJ, Volkening K, Hammond R, Yang W, Strong W, Leystra-Lantz C, et al. TDP43 is a human low molecular weight neurofilament (hNFL) mRNA-binding protein. Mol Cell Neurosci 2007; 35: 320–7.

Swarup V, Phaneuf D, Bareil C, Robertson J, Rouleau GA, Kriz J, et al. Pathological hallmarks of amyotrophic lateral sclerosis/frontotemporal lobar degeneration in transgenic mice produced with TDP-43 genomic fragments. Brain 2011; 134: 2610–26.

Tashiro Y, Urushitani M, Inoue H, Koike M, Uchiyama Y, Komatsu M, et al. Motor neuron-specific disruption of proteasomes, but not autophagy, replicates amyotrophic lateral sclerosis. J Biol Chem 2012; 287: 42984–94.

Tian F, Morimoto N, Liu W, Ohta Y, Deguchi K, Miyazaki K, et al. In vivo optical imaging of motor neuron autophagy in a mouse model of amyotrophic lateral sclerosis. Autophagy 2011; 7: 985–92.

Tollervey JR, Curk T, Rogelj B, Briese M, Cereda M, Kayikci M, et al. Characterizing the RNA targets and position-dependent splicing regulation by TDP-43. Nat Neurosci 2011; 14: 452–8.

Tsai KJ, Yang CH, Fang YH, Cho KH, Chien WL, Wang WT, et al. Elevated expression of TDP-43 in the forebrain of mice is sufficient to cause neurological and pathological phenotypes mimicking FTLD-U. J Exp Med 2010; 207: 1661–73.

Uchida A, Sasaguri H, Kimura N, Tajiri M, Ohkubo T, Ono F, et al. Non-human primate model of amyotrophic lateral sclerosis with cytoplasmic mislocalization of TDP-43. Brain 2012; 135: 833–46.

Wang HY, Wang IF, Bose J, Shen CK. Structural diversity and functional implications of the eukaryotic TDP gene family. Genomics 2004; 83: 130–9.

Wegorzewska I, Bell S, Cairns NJ, Miller TM, Baloh RH. TDP-43 mutant transgenic mice develop features of ALS and frontotemporal lobar degeneration. Proc Natl Acad Sci USA 2009; 106: 18809–14.

Wils H, Kleinberger G, Janssens J, Pereson S, Joris G, Cuijt I, et al. TDP-43 transgenic mice develop spastic paralysis and neuronal inclusions characteristic of ALS and frontotemporal lobar degeneration. Proc Natl Acad Sci USA 2010; 107: 3858–63.

Wu LS, Cheng WC, Hou SC, Yan YT, Jiang ST, Shen CK. TDP-43, a neuro-pathosignature factor, is essential for early mouse embryogenesis. Genesis 2010; 48: 56–62.

Wu LS, Cheng WC, Shen CK. Targeted Depletion of TDP-43 Expression in the spinal cord motor neurons leads to the development of Amyotrophic Lateral Sclerosis (ALS)-like phenotypes in mice. J Biol Chem 2012; 287: 27335–44.

Xu YF, Gendron TF, Zhang YJ, Lin WL, D'Alton S, Sheng H, et al. Wild-type human TDP-43 expression causes TDP-43 phosphorylation, mitochondrial aggregation, motor deficits, and early mortality in transgenic mice. J Neurosci 2010; 30: 10851–9.

Yokoseki A, Shiga A, Tan CF, Tagawa A, Kaneko H, Koyama A, et al. TDP-43 mutation in familial amyotrophic lateral sclerosis. Ann Neurol 2008; 63: 538–42.

Zhang B, Tu P, Abtahian F, Trojanowski JQ, Lee VM. Neurofilaments and orthograde transport are reduced in ventral root axons of transgenic mice that express human SOD1 with a G93A mutation. J Cell Biol 1997; 139: 1307–15.

Zhou H, Huang C, Chen H, Wang D, Landel CP, Xia PY, et al. Transgenic rat model of neurodegeneration caused by mutation in the TDP gene. PLoS Genet 2010; 6: e1000887.

# *dnc-1/dynactin 1* Knockdown Disrupts Transport of Autophagosomes and Induces Motor Neuron Degeneration

**Kensuke Ikenaka**[1], **Kaori Kawai**[1], **Masahisa Katsuno**[1], **Zhe Huang**[1], **Yue-Mei Jiang**[1], **Yohei Iguchi**[1], **Kyogo Kobayashi**[2], **Tsubasa Kimata**[2], **Masahiro Waza**[1], **Fumiaki Tanaka**[1], **Ikue Mori**[2], **Gen Sobue**[1,3]*

1 Department of Neurology, Nagoya University Graduate School of Medicine, Nagoya, Japan, 2 Group of Molecular Neurobiology, Nagoya University Graduate School of Science, Nagoya, Japan, 3 Core Research for Evolutional Science and Technology (CREST), Japan Science and Technology Agency (JST), Saitama, Japan

## Abstract

Amyotrophic lateral sclerosis (ALS) is a fatal neurodegenerative disease characterized by the progressive loss of motor neurons. We previously showed that the expression of dynactin 1, an axon motor protein regulating retrograde transport, is markedly reduced in spinal motor neurons of sporadic ALS patients, although the mechanisms by which decreased dynactin 1 levels cause neurodegeneration have yet to be elucidated. The accumulation of autophagosomes in degenerated motor neurons is another key pathological feature of sporadic ALS. Since autophagosomes are cargo of dynein/dynactin complexes and play a crucial role in the turnover of several organelles and proteins, we hypothesized that the quantitative loss of dynactin 1 disrupts the transport of autophagosomes and induces the degeneration of motor neuron. In the present study, we generated a *Caenorhabditis elegans* model in which the expression of DNC-1, the homolog of dynactin 1, is specifically knocked down in motor neurons. This model exhibited severe motor defects together with axonal and neuronal degeneration. We also observed impaired movement and increased number of autophagosomes in the degenerated neurons. Furthermore, the combination of rapamycin, an activator of autophagy, and trichostatin which facilitates axonal transport dramatically ameliorated the motor phenotype and axonal degeneration of this model. Thus, our results suggest that decreased expression of dynactin 1 induces motor neuron degeneration and that the transport of autophagosomes is a novel and substantial therapeutic target for motor neuron degeneration.

## Introduction

Autophagy is one of the major cellular systems that regulate protein degradation and organelle turnover in physiological and pathological conditions [1], and it is an essential quality control system for proteins in post-mitotic neurons that need to eliminate abnormal proteins and organelles for their proper function and survival [2,3]. It is well known that the dysregulation of autophagy causes neurodegeneration [4,5] and that the abnormal accumulation of autophagosomes is observed in several neurodegenerative diseases [6–9]. Particularly, intensified immunoreactivity for microtubule-associated protein 1 light chain 3 (LC3), which is a marker of autophagosome, is often observed in the spinal motor neurons of amyotrophic lateral sclerosis (ALS) patients [8,10]. Electron microscopy of the motor neurons of ALS patients shows an increased number of autophagosomes surrounded by a double-membrane that contain sequestered cytoplasmic organelles, e.g., mitochondria [8]. Although these observations suggest the possibility that autophagy is upregulated to protect neurons from increased amounts of aggregated proteins and/or damaged

organelles, it is also possible that the accumulation of autophagosomes due to dysregulated autophagy leads to neurodegeneration.

One possible mechanism for the accumulation of autophagosomes in degenerated neurons is the disruption of the cellular transport system, given that autophagosomes are cargo that moves bidirectionally along microtubules, which is powered by the kinesin family of motor proteins and dynein/dynactin complexes [11,12]. We previously investigated the motor neuron-specific gene expression profile of sporadic ALS (SALS), which accounts for more than 90% of ALS, and found that the expression of dynactin 1, which is a key member of the dynactin family, is markedly decreased in the spinal motor neurons of SALS patients [9]. The decreased expression of dynactin 1 was also verified quantitatively using *in situ* hybridization analysis of tissues from SALS patients [13]. By contrast, the expression of other motor proteins including the kinesin family, which are responsible for anterograde transport and dyneins, which are responsible for retrograde transport was not significantly changed. Thus, we hypothesized that the decreased expression of dynactin 1 results in the disrupted transport of autophagosomes and thus attenuates the protective effects of autophagy against neurodegeneration.
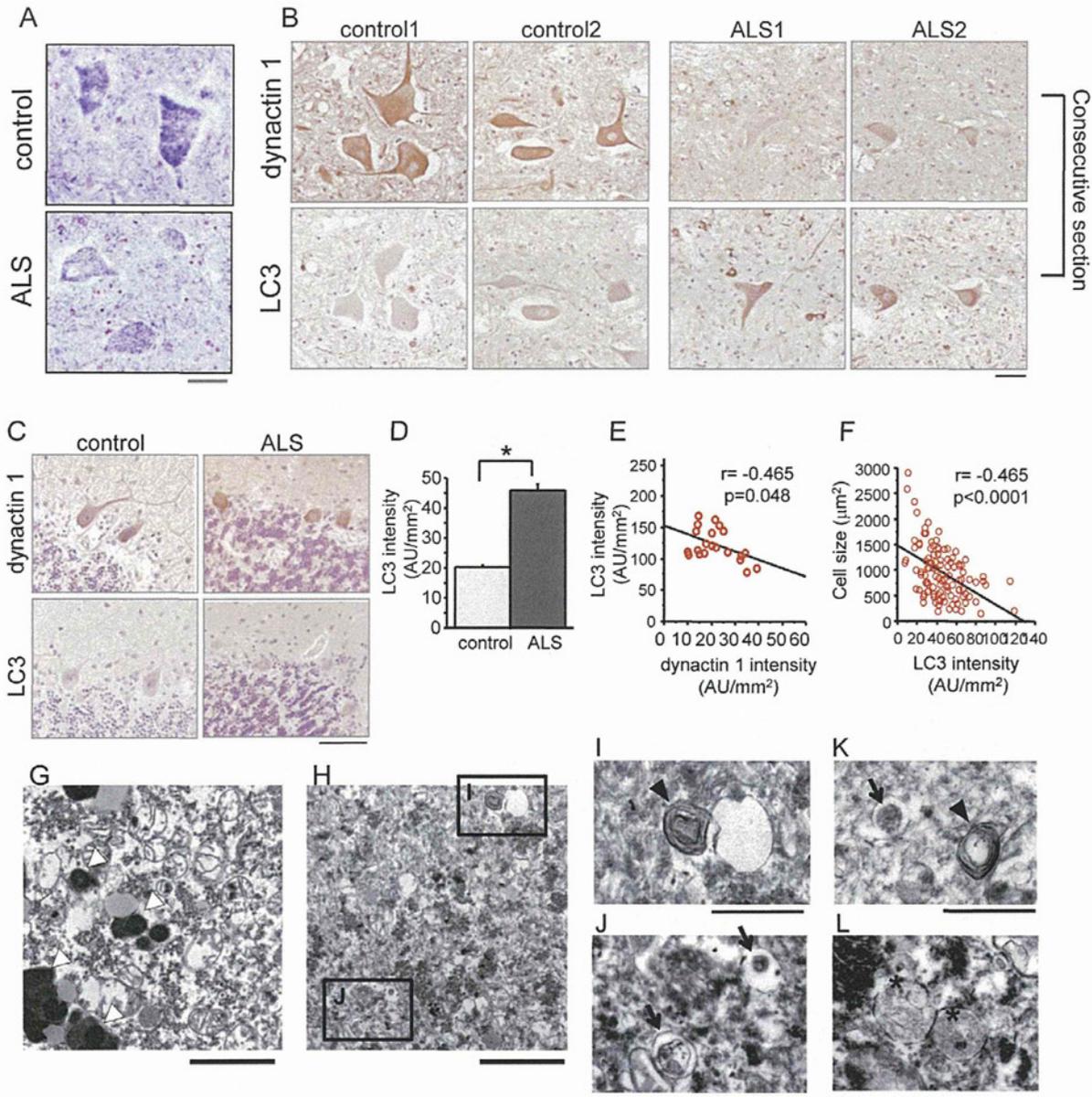
**Figure 1. Dysregulated expression of dynactin 1 and the accumulation of autophagosomes in SALS patients.** (A) Representative *in situ* hybridization for *DCTN1* in the spinal cords of control and ALS patients. (B, C) Representative immunohistochemistry for dynactin 1 and microtubule-associated protein 1 light chain 3 alpha (LC3) on consecutive spinal cord (B) and cerebellar (C) sections from control and ALS patients. (D) Quantification of the signal intensity of LC3 in anterior horn neurons of the spinal cord (n = 20 sections from 4 patients for each group). (E) Correlation between LC3 intensity and the expression of *DCTN1* in individual motor neurons from SALS patients (n = 12 consecutive sections from 3 SALS patients). (F) Correlation between the intensity of LC3 immunoreactivity and the size of motor neurons in SALS patients (n = 20 sections from 4 patients). (G–L) Electron microscopy images of spinal motor neurons. Representative lower magnification image of a motor neuron from a control patient (G) and lower (H) and higher magnification images (I–L) from SALS patients. The open arrowheads indicate lipofuscin. There were abundant autophagic vacuoles, e.g., multi-lamellar bodies (arrowheads in I, K), autophagosome-like double membrane vesicles (arrows in K, J), and autolysosomes (asterisks in L) in the motor neurons of SALS patients, but not of the control. Scale bar = 50 μm (A–C), 2 μm (G, H), or 1μm (I–L). Statistical analyses were performed using Student's t test (*p<0.0001) and Pearson's correlation coefficient in E and F. The error bars are S.E.M.
doi:10.1371/journal.pone.0054511.g001

Moreover, mutations of *DCTN1*, the gene encoding dynactin 1, are linked to familial lower motor neuron disease [14]. Several mutant *DCTN1* models exhibited motor dysfunction and pathological changes related to motor neuron disease [15,16]. As seen in the motor neurons of SALS patients, mutant *DCTN1* mice exhibited a massive accumulation of membrane vesicles, including autophagosomes, in spinal motor neurons [16]. Although these findings suggest that impaired vesicular trafficking might cause the

accumulation of vesicles, it remains unclear whether the transport of autophagosomes is actually impaired in the mutant *DCTN1* mice or whether the accumulation of autophagosomes plays a causative role in the pathogenesis of motor neuron degeneration.

The aim of the present study was to clarify the biological link between the quantitative loss of dynactin 1 and the disruption of autophagy. In particular, we examined whether the decreased levels of dynactin 1 induce motor neuron degeneration by
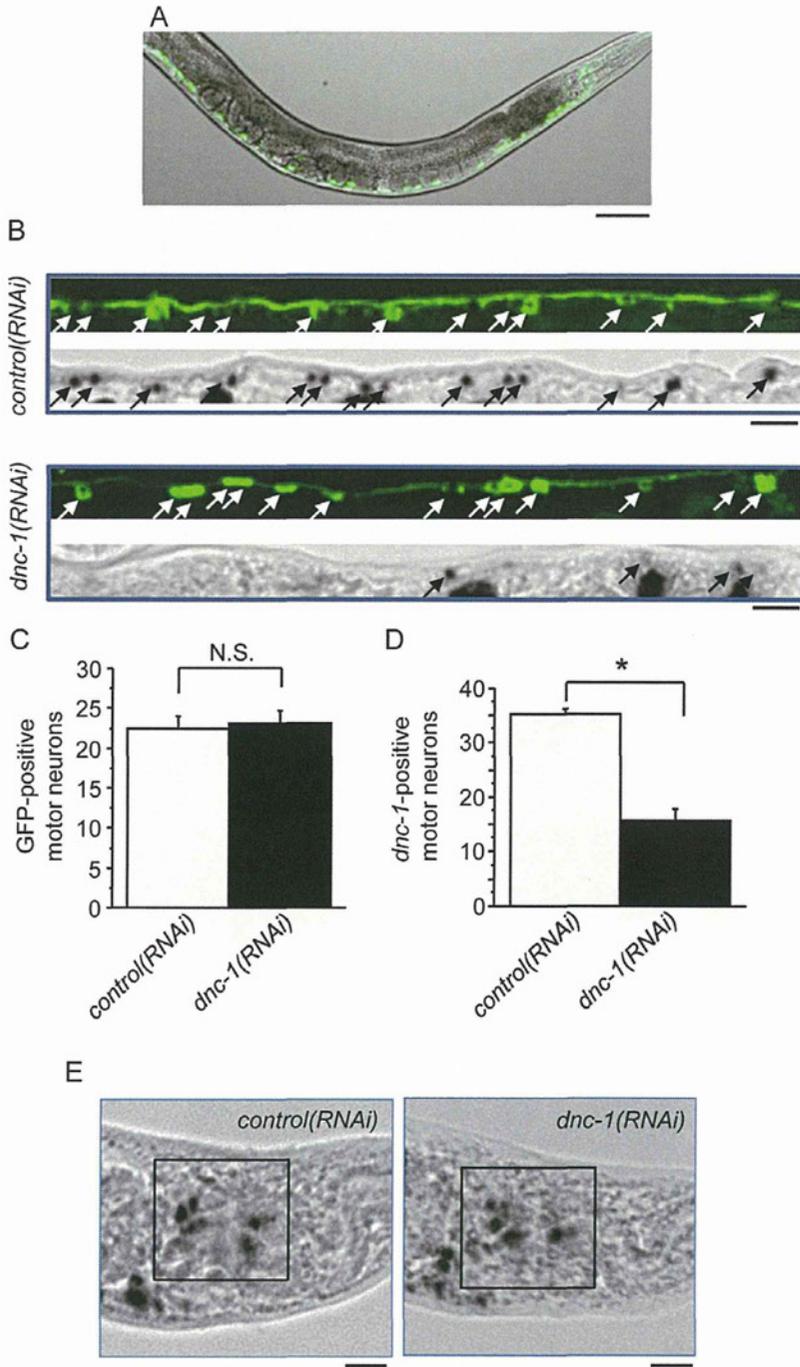
**Figure 2. Creation of the motor neuron-specific *dnc-1*-KD *C. elegans* model.** (*A*) Fluorescent visualization of ventral cholinergic motor neurons and their neurites in transgenic *C. elegans* worms expressing acr2p::shRNA::gfp. (*B*) Representative immunohistochemical staining of GFP and *in situ* hybridization against *dnc-1* in ventral cholinergic motor neurons and their neurites in the *control(RNAi)* and *dnc-1(RNAi)* worms. (*C*) The number of GFP-positive motor neurons (white arrows in *B*) was not significantly different between the *control(RNAi)* and *dnc-1(RNAi)* worms (n = 20 animals for each strain). (*D*) Conversely, the number of *dnc-1* mRNA-positive neurons (black arrows in *B*) was remarkably decreased in the *dnc-1(RNAi)* worms (n = 20 animals for each strain). (*E*) Representative images of *in situ* hybridization for *dnc-1* in the head neurons. Scale bars = 100 μm (*A*), 10 μm (*B*), and 20 μm (*E*). Statistical analyses were performed using Student's t test (*p<0.0001). The error bars are S.E.M.
doi:10.1371/journal.pone.0054511.g002

hindering the transport of autophagosomes. To this end, we first examined the relationship between the decreased levels of dynactin 1, the accumulation of autophagosomes, and motor neuron degeneration in post-mortem tissues from SALS patients. Next, we created a *Caenorhabditis elegans (C. elegans)* model of the motor neuron-specific knockdown (KD) of *dnc-1*, the *C. elegans*

homolog of human *DCTN1*, using small hairpin RNA (shRNA), and investigated whether the depletion of dynactin 1 impairs the transport of autophagosomes and thereby induces motor neuron degeneration. Using this model, we also explored therapeutic strategies targeting the transport of autophagosomes.

- 124 -
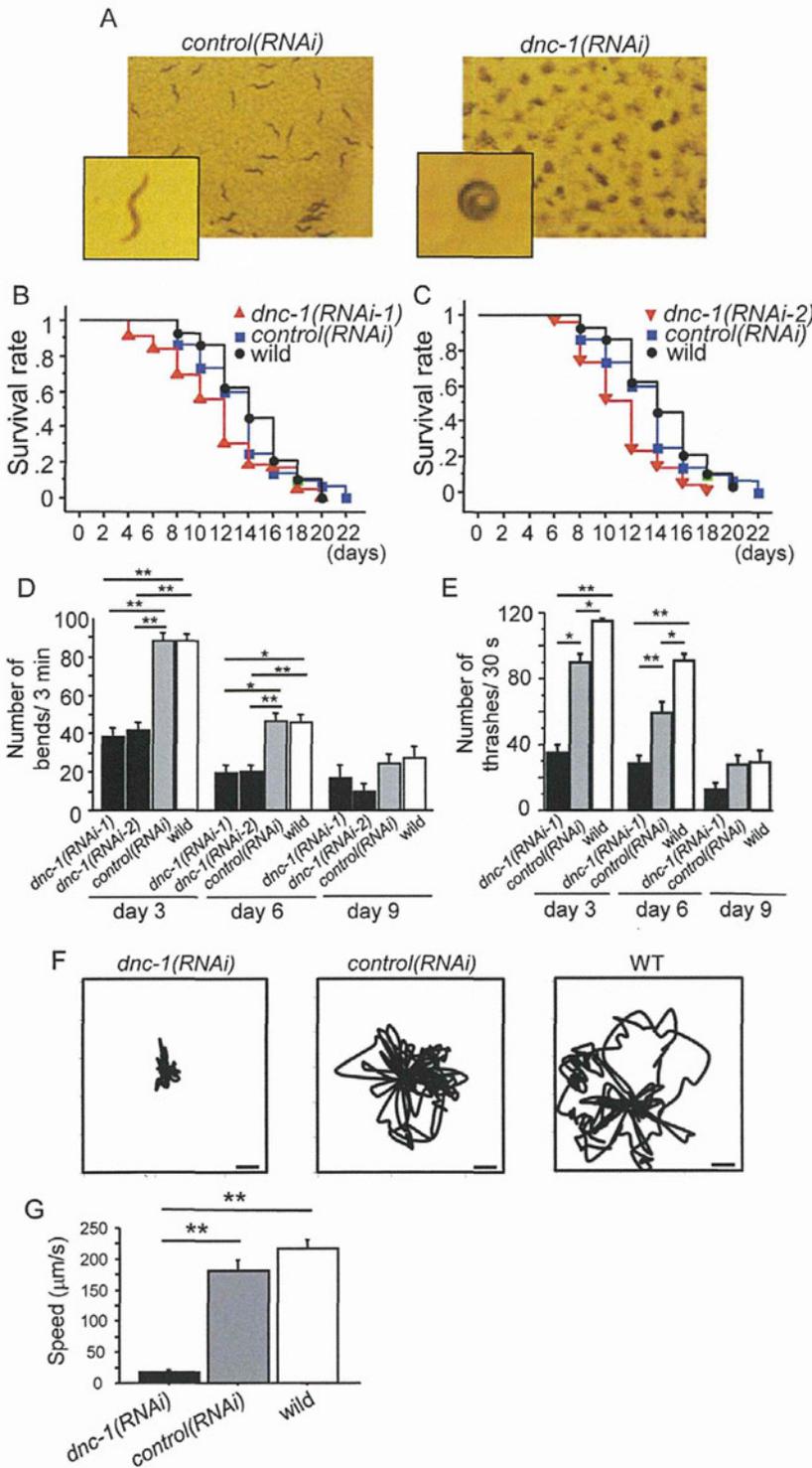
**Figure 3. Motor dysfunction in the motor neuron-specific *dnc-1*-KD *C. elegans* model.** (A) Stereoscopic microscopy showing the phenotypes of the *control(RNAi)* and *dnc-1(RNAi)* worms. (B, C) Survival curves of the transgenic worms (*dnc-1(RNAi-1)*, n = 90; *dnc-1(RNAi-2)*, n = 90; *control(RNAi)* n = 90; and wild-type n = 30). The same survival data of the *control(RNAi)* and wild-type worms were used in both graphs. Both *dnc-1(RNAi)* worms with different shRNA sequences (101, 2888) had significantly reduced life spans compared with the *control(RNAi)* worms (101: p = 0.005; 2888: p<0.0001; log-rank test). (D) The number of body bends associated with forward movement in 3 min. (E) The number of thrashing movements in liquid medium in 30 s. (F, G) The tracks (F) and average speed of the worms (G) analyzed by video capture at day 4. Scale bars in F = 100 μm. The error bars are S.E.M. (n = 30, 30, 40, and 40 for *dnc-1(RNAi-1)*, *dnc-1(RNAi-2)*, *control(RNAi)*, and wild-type, respectively, in D, E; and n = 6, 6, and 6 for *dnc-1(RNAi-1)*, *control(RNAi)*, and wild-type, respectively, in G). The statistical analyses in C, D, and F were performed by one-way ANOVA followed by the Bonferroni/Dunn post hoc test (*p<0.001 and **p<0.0001).
doi:10.1371/journal.pone.0054511.g003

## Materials and Methods

### Protocols for the human samples

**Ethics Statement.** The collection of autopsied human tissues and their use for this study were approved by the Ethics Committee of Nagoya University Graduate School of Medicine, and written informed consent was obtained from the patients' next-of-kin. Experimental procedures involving human subjects were conducted in conformance with the principles expressed in the Declaration of Helsinki.

**Immunohistochemistry.** Six micrometer-thick sections from paraffin-embedded spinal cord sections from autopsied patients were prepared as described previously [17]: four patients with sporadic ALS (64.5±9.3 years-old; M:F = 2:2) and four disease controls (73.5±5.4 years-old; M:F = 1:3). The four control patients were diagnosed with progressive supranuclear palsy, multiple system atrophy, diffuse lewy body disease, and Parkinon's disease, respectively. The sections were first microwaved for 20 min in 50 mM citrate buffer, pH 6.0, then blocked with TNB blocking buffer (PerkinElmer, Hvidovre, Denmark) in Tris-
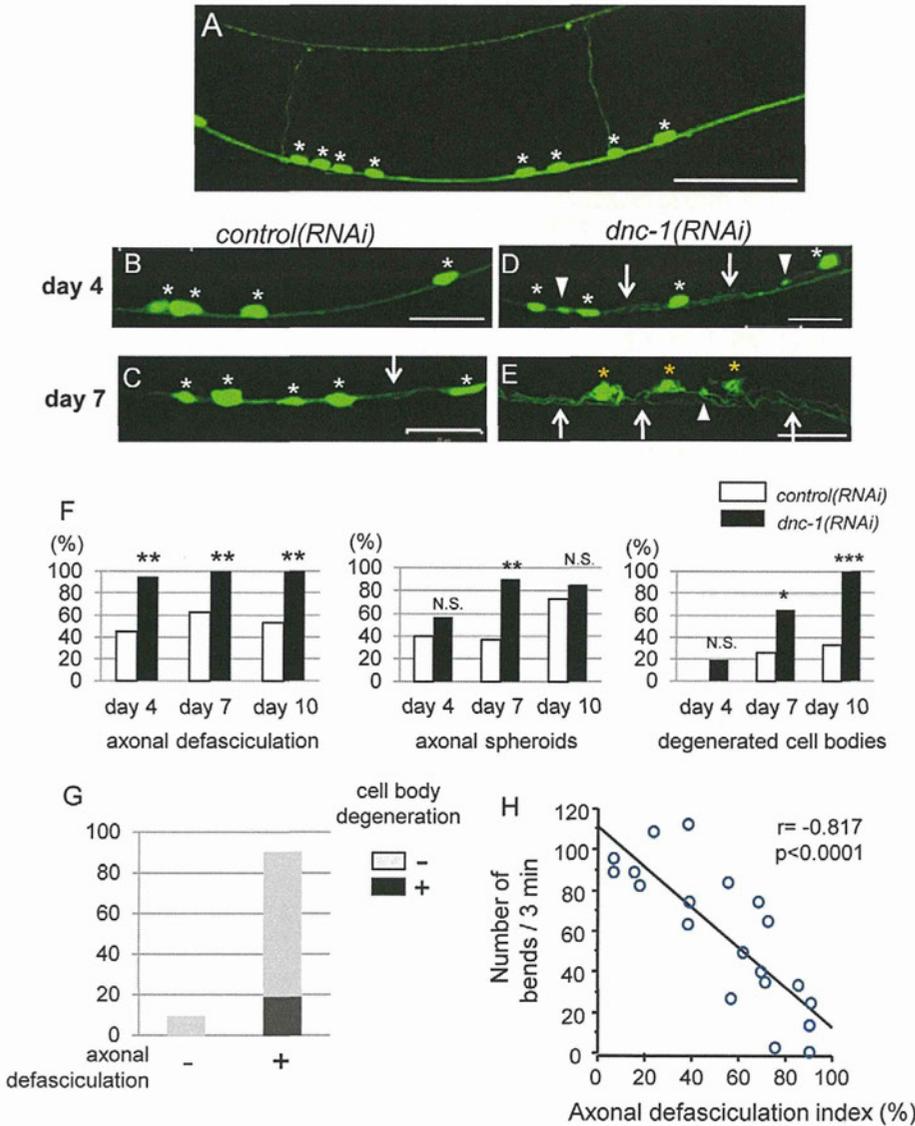


**Figure 4. Morphological changes in ventral motor neurons.** (A) Representative view of fluorescent GFP microscopic images of the ventral nerve cord in a *control(RNAi) C. elegans*. All of the motor neurons (white asterisks) were located in the ventral side of the worm. Axons from the motor neurons project within the ventral nerve cord or toward the dorsal side. (B–E) Representative view of the ventral nerve cord in the *control(RNAi)* worms (B, C) and *dnc-1(RNAi)* worms (D, E). The degenerated axons were defasciculated (arrows in D, E) and formed spheroids (arrowheads in D, E) in the *dnc-1(RNAi)* worms. Mild defasciculation was observed occasionally in the *control(RNAi)* worms (arrow in C). While the cell bodies of the motor neurons were regular and round in *control(RNAi)* and young adult *dnc-1(RNAi)* worms (white asterisks in B–D), abnormally shaped cell bodies (yellow asterisks in E) were observed only in the worms with severe axonal changes. (F) Semi-quantification of the abnormal morphological changes in the *control(RNAi)* and *dnc-1(RNAi)* worms. The percentage of worms with axonal defasciculation, axonal spheroids, or cell body degeneration on days 4, 7, and 10. (G) Population of *dnc-1(RNAi)* worms with and without cell body degeneration (black and gray boxes, respectively) on day 4. (H) Correlation between the axonal defasciculation index and locomotor function in the *dnc-1(RNAi)* worms. The axonal defasciculation index represents the degree of axonal defasciculation (its details are described in the Materials and Methods). Scale bars = 20 μm. The statistical analysis in F was performed using Fisher's exact probability test (*p<0.05, **p<0.001, and ***p<0.0001) and Pearson's correlation coefficient in H.
doi:10.1371/journal.pone.0054511.g004

- 126 -

buffered saline (pH 7.5) at room temperature for 30 min and incubated with a monoclonal antibody against LC3 (anti-LC3, 1:40000; Medical & Biological Laboratories, Co., Nagoya, Japan) or dynactin 1 (anti-dynactin 1 H300; 1:2000; Santa Cruz, Santa Cruz, CA, USA) overnight at 4°C. The subsequent procedures were carried out using the EnVision+Kit/HRP (DAB) (DAKO, Glostrup, Denmark) according to the manufacturer's protocol.

**Quantitative assessment of immunohistochemistry.** To assess LC3 immunoreactivity in spinal motor neurons, we included 4 ALS patients and 4 disease controls, and prepared 5 independent specimens from each subject. We counted about 200 motor neurons in ALS patients and about 400 neurons in control patients. The intensity of immunohistochemistry signals was quantified using a BZ-8000 fluorescent microscope and its software (BZ-Analyzer; Keyence, Osaka, Japan). Signal intensity was expressed as the individual intracellular cytoplasmic signal level (arbitrary absorbance units/mm$^2$) per motor neuron by subtracting the mean background levels of 3 regions of interest in each section. The ventral spinal horn was defined as the gray matter ventral to the line through the central spinal canal perpendicular to the ventral spinal sulcus. To investigate the correlation between dynactin 1 and LC3 in individual motor neurons we used consecutive transverse spinal cord sections.

*In situ* **hybridization.** *In situ* hybridization for human tissue was performed as described previously [13]. We provide the detailed information in Materials and Methods S1.

**Electron microscopy.** Electron microscopy was performed on samples from 2 sporadic ALS patients (71 years-old male and 62 years-old female) and 2 disease control patients (68 years old male with multiple system atrophy and 60 years-old male with multiple system atrophy). Epoxy resin-embedded specimens of spinal anterior horn were cut into 70-nm ultrathin sections. Ultrathin sections were contrasted by staining with uranyl acetate

and lead citrate. Sections were viewed with a JEM-1400EX electron microscope (JEOL, Tokyo, Japan) at 80 kV.

## Protocols for *C. elegans*

**Ethics statement.** All animal experiments were performed in accordance with the National Institute of Health Guide for the Care and Use of Laboratory Animals and were approved by the Nagoya University Animal Experiment Committee.

**Culture of *C. elegans*.** Standard methods were used to culture *C. elegans* on nematode growth medium (NGM) agar [18]. The animals were maintained at 20°C unless otherwise indicated. We provide the detailed information in Materials and Methods S1.

**Constructs and *C. elegans* Strains.** To generate transgenic *C. elegans*, plasmid DNA encoding acr2promotor::*shRNA*::*gfp* was injected into the gonads of young adult hermaphrodite N2 worms. We provide the detailed information for the shRNA vector and other co-injected proteins, i.e., SNB-1 and Lgg1, in Materials and Methods S1.

**Whole Mount *in situ* Hybridization.** Whole mount *in situ* hybridization of worms was performed as described previously [13,19]. We provide the detailed information in Materials and Methods S1.

**Phenotypic analysis of *C. elegans*.** A lifespan assay was performed as described preciously [20], with some modifications. The Worms were allowed to lay eggs on a dish for 3–6 h to obtain synchronous progeny for the experiment. L4 worms were collected and transferred every 3 days to a fresh plate until the end of their reproductive life. The animals were scored as dead if they did not move when prodded with a platinum pick and did not show pharyngeal pumping.

A body bend assay, liquid thrashing assay, and video capture analysis were performed as locomotion assays. To examine the body bend frequency, exposed worms were transferred onto a fresh NGM plate and scored for the number of body bends



Nu: nucleus, M: muscle, W: whorl-like inclusion, V: vacuole
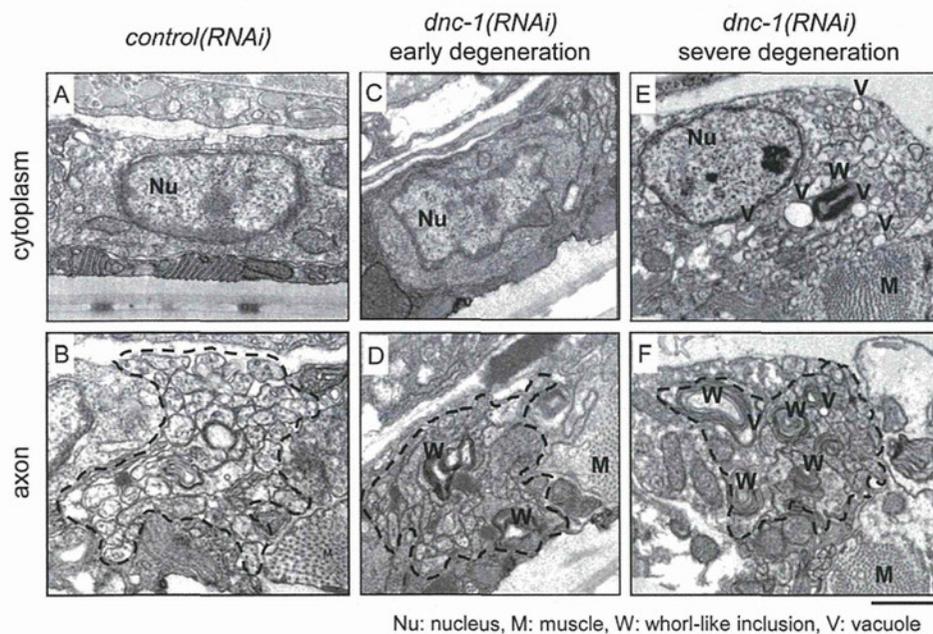
**Figure 5. Ultrastructure of degenerating motor neurons.** Electron microscopy of transverse sections of ventral motor neurons from the *control(RNAi)* (A, B) and *dnc-1(RNAi)* (C–F) worms. The dashed lines in B, D, and F denote the boundaries of the main bundle of axons. Each round-shaped component inside the dashed line is an axon. In the *dnc-1(RNAi)* worms, whorl-like inclusions (W) and vacuoles (V) were observed (D–F). In the worms with mild axonal degeneration (D), few morphological changes were observed in the cytoplasm (C); however, in the later stage with severe axonal degeneration (F), the cell bodies were also affected (E). Scale bars = 20 µm.
doi:10.1371/journal.pone.0054511.g005

- 127 -
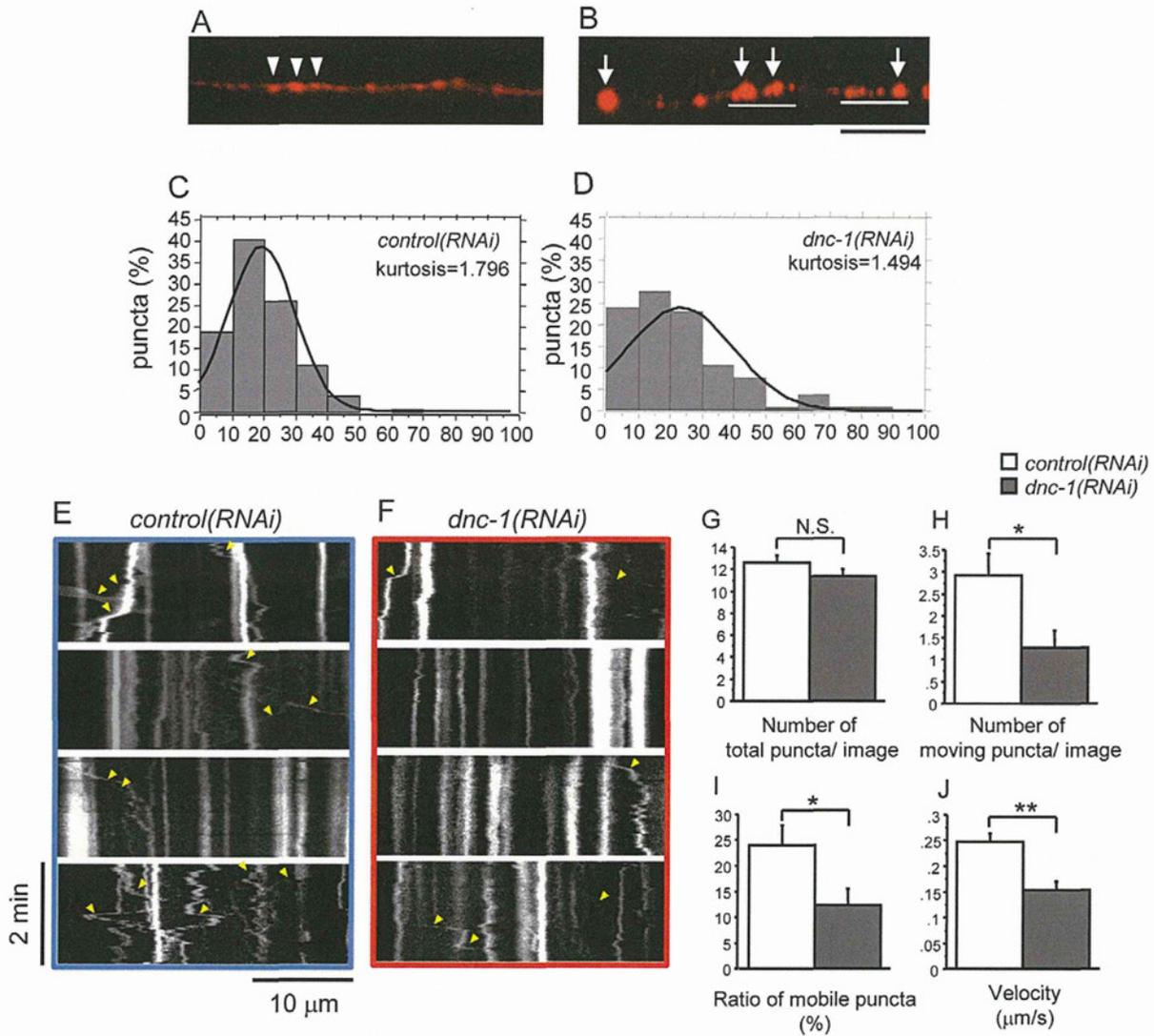
**Figure 6. Defective axonal transport of synaptobrevin-1 in *dnc-1(RNAi)* C. elegans.** (A, B) Expression patterns of DsRed-tagged synaptobrevin-1 (SNB-1) in the dorsal nerve cord. In the *control(RNAi)* worms, SNB-1 puncta (arrowheads) are regularly spaced with a uniform shape. In the *dnc-1(RNAi)* worms (B), they are irregularly spaced and abnormally accumulated (white bars) with occasional clumps. (C, D) Histograms of the distances between neighboring SNB-1 puncta. The average distance between puncta in the *control(RNAi)* (3.240±1.716 µm, n = 139) and *dnc-1(RNAi)* (3.855±2.764 µm, n = 104) worms was not significantly different (p = 0.996 by Student's t test), but the peak of the control histogram was higher than that of the *dnc-1(RNAi)* histogram, proving that the localization of SNB1 was irregular. (E, F) Representative kymographs of SNB-1::DsRed in the ventral nerve cord from the *control(RNAi)* (E) and *dnc-1(RNAi)* (F) worms derived from time-lapse imaging. Vertical lines represent stationary/docked SNB-1 puncta and oblique lines (labeled with yellow arrowheads) represent the tracks of moving SNB-1 puncta. The slope of this track is an indicator of velocity. (G) The number of SNB-1 puncta within a single image of kymograph was not different between the *control(RNAi)* and the *dnc-1(RNAi)* worms. (H) The mean velocities of SNB-1 puncta. (I, J) The quantitative analysis of mobile puncta. The number of puncta which moved more than 2 µm was counted (I). The ratio of moving puncta was calculated by dividing the number of moving puncta by the total number of SNB-1 puncta (J). A total of 20 time laps images were analyzed from each strains in G–J. Scale bar (black) = 10 µm (B). Statistical analyses were performed using Student's t test (*p<0.05, **p<0.001, ***p<0.0001). Error bars are S.E.M.
doi:10.1371/journal.pone.0054511.g006

performed in 3 min. A body bend was defined as a change in the direction of the part of the worm corresponding to the posterior bulb of the pharynx along the y-axis, assuming that the worm was traveling along the x-axis. We also performed a liquid thrashing assay as described previously [21], with some modifications. Briefly, the worms were put on a 6-cm NGM-coated plate with 3 ml of M9 media. The worms were allowed to settle for 30 s, their movements were captured by video for 30 s, and the number of thrashing movements was counted. We also analyzed the speed of movement using a video capture system as described previously [22]. Briefly, fully matured, adult worms were transferred

individually to agar plates with no food. The movement of each worm was observed for 5 min and recorded using video equipment (Olympus, Tokyo, Japan) with a sampling rate of 30 frames/s. A computer-controlled microscope stage was automatically moved to center the worms in the visual field using a custom image analysis algorithm within the microscope's software package (MetaMorph; Universal Imaging Corp., West Chester, PA, USA). The midlines of the recorded worms were extracted from each image. All strains were randomized and scored on the same day.

- 128 -
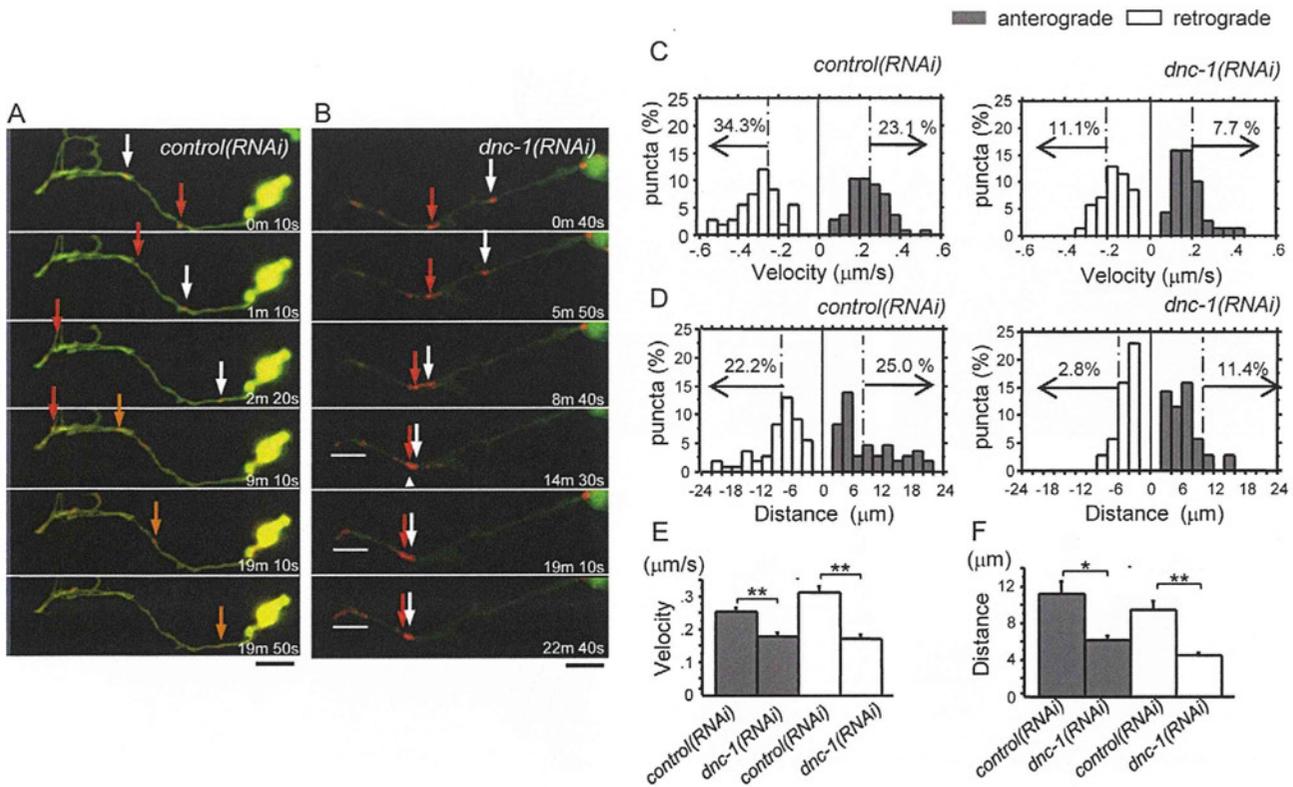
**Figure 7. Impaired transport and abnormal accumulation of autophagosomes in the axons of *dnc-1(RNAi)* motor neurons.** (A, B) Representative time-lapse images of autophagosome (DsRed-tagged Lgg1) transport in an axon (GFP-tagged shRNA; green) of a primary cultured motor neuron from the *control(RNAi)* (A) and *dnc-1(RNAi)* (B) worms. The autophagosomes were transported smoothly along the axon (arrows) of the *control(RNAi)* motor neuron (A). The autophagosome (arrows) was transported anterogradely, but was trapped where the axon was slightly narrowed (arrowhead) (B). There were also autophagosomes that accumulated in the distal part of the axon (B, bar). (C) Histograms of Lgg1::DsRed velocity in the retrograde (white bars) and anterograde (black bars) directions in neurons from the *control(RNAi)* and *dnc-1(RNAi)* worms. (D) Histograms of Lgg1::DsRed run-length in the *control(RNAi)* and *dnc-1(RNAi)* neurons. (E, F) Mean velocity (E) and run-length (F) of autophagosomes (n = 70 vesicles for each strain) in *control(RNAi)* and *dnc-1(RNAi)* neurons. Scale bar = 5 μm (A and B). The statistical analyses in E and F were performed using the Mann-Whitney U test (*p<0.05 and **p<0.0001). The error bars are S.E.M.
doi:10.1371/journal.pone.0054511.g007

**Preparation of starved worms for the dietary restriction assay.** All worms were synchronized by egg preparation [23]. The eggs were incubated at 20°C for 48 h in liquid medium. After 48 h, newly hatched worms were washed 3 times with distilled water, transferred to S basal medium without OP50, and incubated for 24 h. Worms were then picked randomly and used for the liquid thrashing assay.

**Drug treatment.** The worms were synchronized by egg preparation and incubated at 20°C for 24 h in liquid medium. They were then treated with rapamycin (LC Laboratories, Woburn, MA, USA) dissolved in ethanol at a final concentration of 10 or 100 μM, 3-methyladenine (3-MA) (SIGMA) dissolved in DMSO at a final concentration of 1 or 10 mM, or trichostatin A (TSA) (Tokyo Chemical Industry, Co., Tokyo, Japan) dissolved in DMSO at a final concentration of 1, 10, or 100 μM and incubated in liquid medium for 48 h. For controls (0 μM), ethanol or DMSO was added. Worms were then picked randomly and used for the liquid thrashing assay or microscopic analysis.

**Primary neuronal cell cultures of nematodes.** Primary neuronal cell cultures were prepared as described previously [24], with some modifications. In the present study, in order to obtain larger number of gravid animals, we cultured the worms in liquid medium (S basal medium with concentrated OP50) as described previously [25]. After incubation in liquid medium for 3 days, we performed egg isolation using lysis buffer (0.5 M NaOH/1%

NaClO). Then we removed eggshell by enzymatic digestion using chitinase (SIGMA) and isolated embryonic cells were plated onto peanut lectin-coated glass bottom dishes (IWAKI, Tokyo, Japan).

**Microscopic analysis.** The worms were anesthetized by placing them in an 8-μl drop of levamisole (2 mM) on solidified pads of 2% agarose laid on slides. After coverslipping, the worms were examined under an LSM710 confocal microscope (Carl Zeiss Inc., Thornwood, NJ, USA). The regularity of SNB-1::DsRed localization/spacing was evaluated by measuring the distance between two neighboring fluorescent puncta of SNB-1::DsRed using ImageJ 1.43 software (National Institutes of Health). The axonal defasciculation index was measured as follows. The ventral nerve cord was divided into compartments consisting of two neighboring motor neurons. We counted the number of compartments with axonal defasciculation and divided it by the total number of compartments.

In vivo analysis of autophagosome mobility was performed as follows. Lgg1::DsRed worms were plated on an agar pad and observed using confocal microscopy. The red puncta, which represent autophagosomes, were observed for 1 min. The number of autophagosomes that moved within 1 min was divided by the total number of autophagosomes observed.

***In vitro* transport assay and image analysis.** Time-lapse images were acquired at room temperature using a 63× oil-immersion objective (N.A 1.4) for live-cultured neuron analysis at

- 129 -
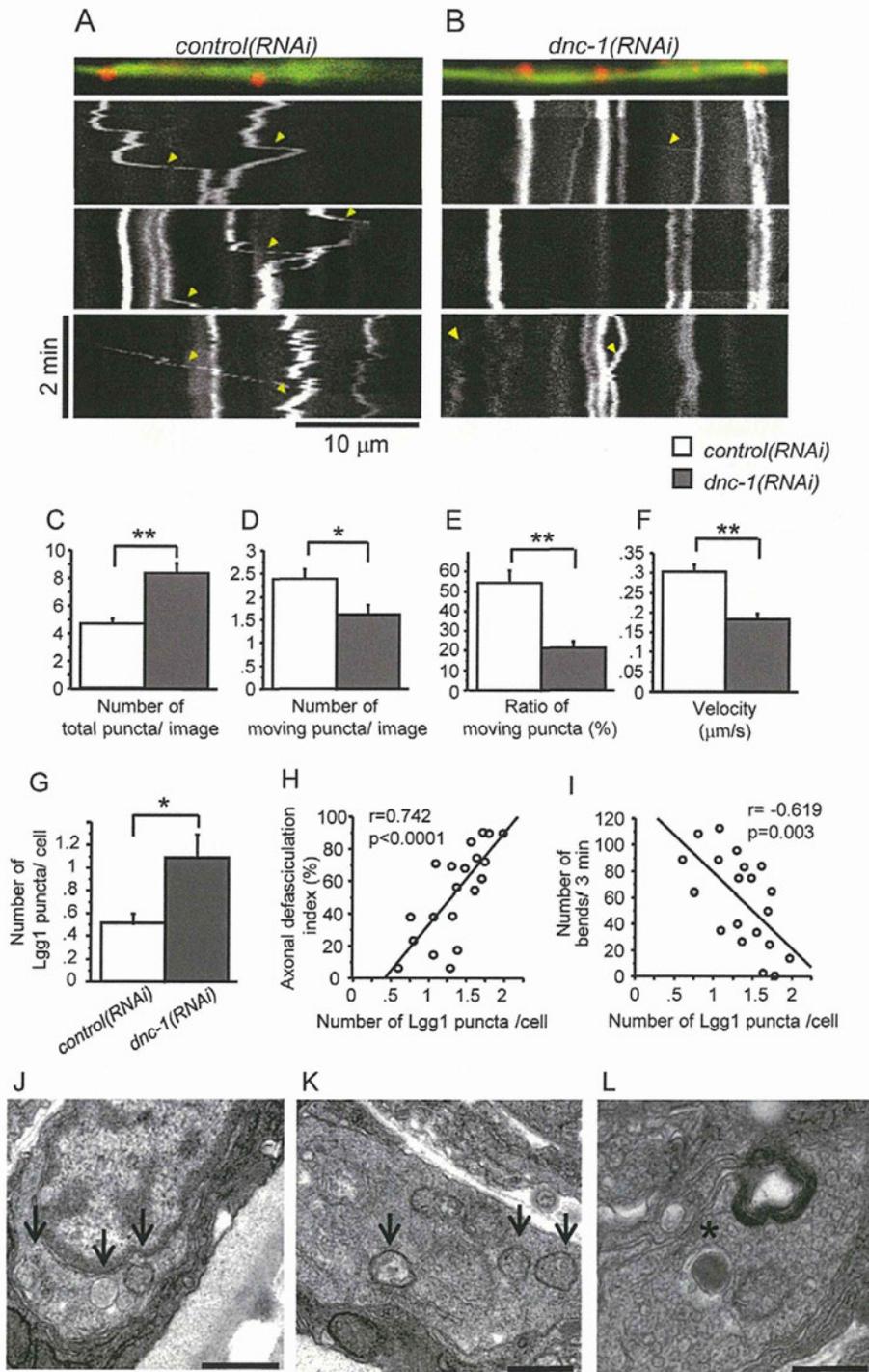
**Figure 8. Accumulation of autophagosomes and motor neuron degeneration in the _dnc-1(RNAi)_ worms.** (A, B) Representative kymographs of Lgg1::DsRed in the ventral nerve cord from the _control(RNAi_ (A) and _dnc-1(RNAi)_ (B) worms derived from time-lapse images. Vertical lines represent stationary/docked Lgg1 puncta, while the oblique lines (labeled with arrowheads) represent the tracks of moving Lgg1 puncta. The slope of this track is an indicator of velocity. (C) The number of Lgg1 puncta within a single kymograph image. (D, E) Quantitative analyses of the mobility of puncta. The number of puncta that moved more than 2 μm was counted (D). The ratio of moving puncta was calculated by dividing the number of moving puncta by the total number of puncta (E). (F) The mean velocities of Lgg1 puncta. A total of 20 time-lapse images were analyzed for each strain in C–F. (G) The number of Lgg1 puncta was increased in the _dnc-1(RNAi)_ worms compared with the _control(RNAi)_ worms (n = 15 for each group). (H, I) Accumulation of autophagosomes in the _dnc-1(RNAi)_ worms was correlated with the severity of axonal defasciculation (H) and locomotor function (I) (n = 20 for each analysis). (J–L) Ultrastructural images of ventral motor neurons from the _dnc-1(RNAi)_ worms. Aberrant membranous vesicles including degenerated mitochondria were observed in the cytoplasm (J) and axons (K) (arrows). Autophagosome-like, double membrane vesicles (asterisk in L) were also found in the axons of the _dnc-1(RNAi)_ worms (L). Scale bar = 500 nm (A–C) or 10 μm (D). Statistical analyses were performed using Student's t test (*p<0.05 and **p<0.0001) and Pearson's correlation coefficient in H and I. The error bars are S.E.M.
doi:10.1371/journal.pone.0054511.g008

- 130 -
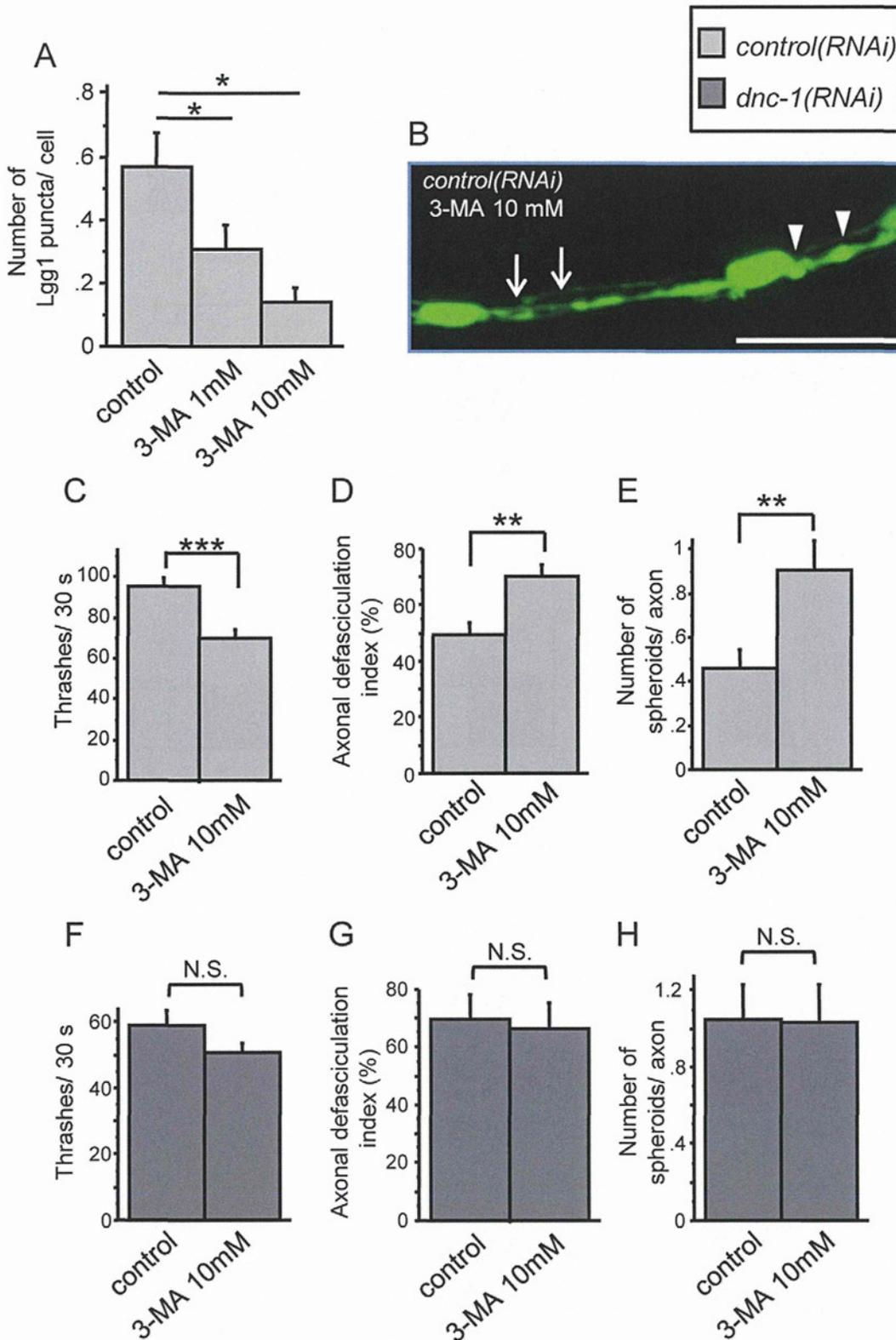
**Figure 9. Dysfunction of autophagy causes axonal degeneration.** (A) Treatment with 3-MA decreased the number of autophagosomes in the ventral nerve cord in a dose dependent manner (n = 15 for each group). (B–E) The effects of 3-MA on the locomotor function (C) and axonal morphology (B, D, and E) of the control(RNAi) worms. Treatment with 3-MA increased axonal defasciculation (arrows in B and the graph in D) and the number of axonal spheroids (arrowheads in B and the graph in E) (n = 15 for each group). (F–H) The effects of 3-MA on the locomotor function (F) and axonal morphology (G, H) of the dnc-1(RNAi) worms (n = 15 for each group). Scale bar = 10 μm. Statistical analyses were performed using Dunnett's post hoc test (A) and Student's t test (B, D, and E) (*p<0.05, **p<0.001, and ***p<0.0001). The error bars are S.E.M.
doi:10.1371/journal.pone.0054511.g009
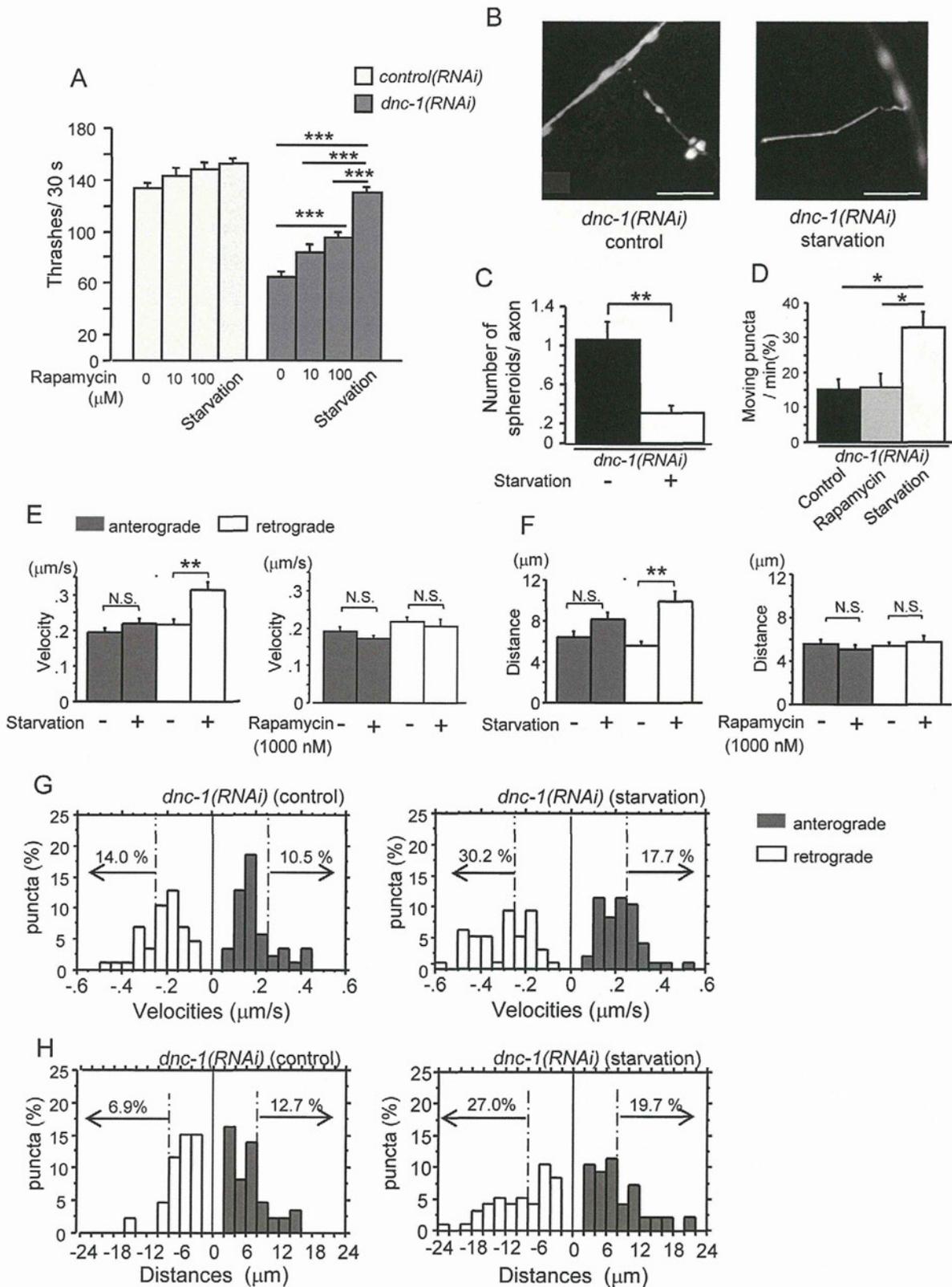
**Figure 10. Starvation stimulates the retrograde transport of autophagosomes and attenuates axonal degeneration in the *dnc-1(RNAi)* worms.** (A) Effect of rapamycin and starvation on locomotor function in the *control(RNAi)* and *dnc-1(RNAi)* worms (n = 50 for each group). (B) Fluorescent microscopy showing the morphological changes in axons after starvation in the *dnc-1(RNAi)* worms. (C) The number of axonal spheroids per transverse axon section in the *dnc-1(RNAi)* worms with or without starvation. (n = 15 animals for each treatment). (D) Effect of rapamycin (100 µM) and starvation on autophagosome mobility in the *dnc-1(RNAi)* worms. (n = 15 animals for each treatment). (E, F) Effect of rapamycin (100 µM) and starvation on the mean velocity (E) and run-length (F) of autophagosomes (black bars: anterograde transport; white bars: retrograde transport) (n = 70

- 132 -

vesicles for each treatment). (*G, H*) Histograms of Lgg1::DsRed velocity (*F*) and run-length (*G*) in the anterograde (black bars) and retrograde (white bars) direction in primary motor neurons from the *dnc-1(RNAi)* worms cultured with normal (control) and serum-free (starvation) medium. Scale bars = 5 μm. Statistical analyses were performed by one-way ANOVA followed by the Bonferroni/Dunn post hoc test (*A*) and Dunnett's post hoc test (*D*). Student's t test (*C*) and Mann-Whitney test (*E, F*) were used for two-group comparison (*p<0.05, **p<0.001, and ***p<0.0001). The error bars are S.E.M.

doi:10.1371/journal.pone.0054511.g010

1–2 frames/s. The images were analyzed using Zen2008 (Zeiss) software. The run-length of Lgg-1 in primary motor neurons was measured by drawing a line over moving fluorescent puncta using Zen2008. Motile puncta were counted only if they moved continuously in the same direction for more than 2 frames and if their displacement was at least 2 μm. Some runs were terminated by a pause or reversal. To ensure the accuracy of the run-length measurements, we excluded moving puncta at the beginning and end of the movie. The velocity of Lgg-1 movements was obtained from the total distance traveled divided by the duration of the run.

**In vivo transport assay and image analysis.** Time-lapse images were acquired at room temperature using a 63× objective (N.A. 1.4) for live-worm analysis at 1 frame/s. The images were analyzed using Image J 1.43 software (National Institutes of Health). First, individual tracks of SNB-1 or Lgg1 movement were analyzed using the Multiple Kymograph plug-in, as described previously [26]. The velocity of the moving vesicles was tracked manually and their instantaneous velocity was extracted. To calculate the ratio of moving versus total vesicles, the number of vesicles that moved more than 2 μm during each time lapse period was divided with the total number of particles in each acquisition.

**Electron microscopy of C. elegans.** A conventional two-step fixation method was performed as described previously [27]. We provide the detail information in Materials and Methods S1.

**Western Blot Analysis and Quantitative real-time PCR.** Western blot analyses and quantitative real-time PCR were performed as described previously [28,29]. We provide a detail description in Materials and Methods S1.

**Statistical analysis.** Statistical analyses were performed using StatView software version 5 (Hulinks, Tokyo, Japan). We used the Kaplan-Meier and log-rank test, Student's t-test, Mann-Whitney U test, and one-way analysis of the variance (ANOVA) with the Bonferroni or Dunnett's post-hoc test. Pearson's correlation coefficient was used to assess the correlation of variables.

## Results

### Dysregulated dynactin 1 expression and autophagy in degenerated spinal motor neurons in SALS patients

The expression of the *DCTN1* gene was markedly reduced in the spinal motor neurons of SALS patients, as reported previously [9,13] (Fig. 1*A*). Recent studies indicate that the dysregulation of autophagy in motor neurons is a pivotal event in ALS [8,10]; thus, we investigated the relationship between decreased dynactin 1 expression and autophagy in SALS. Immunohistochemistry using consecutive sections of autopsied human spinal cords revealed that LC3 immunoreactivity, a histological marker of autophagy, was increased in the motor neurons of SALS patients in which dynactin 1 expression was decreased (Fig. 1*B*). Conversely, there was no change in the immunoreactivity for dynactin 1 and LC3 in cerebellar Purkinje cells, which showed no degeneration (Fig. 1*C*). Quantitative analysis revealed that anti-LC3 immunoreactivity was significantly increased in the spinal motor neurons of SALS patients (p<0.0001) (Fig. 1*D*), and was inversely correlated with the decreased mRNA levels of *DCTN1* (Fig. 1*E*) and cell size

(Fig. 1*F*) in the motor neurons of SALS patients, indicating that the dysregulation of autophagy is associated with the decreased expression of dynactin 1 in SALS. Electron microscopy of sections from the SALS and control patients (Fig. 1*G, H*) also revealed that there was an abundance of autophagic vacuoles, e.g., multi-lamellar bodies (arrowheads in Fig. 1*I, K*), autophagosome-like double membrane vesicles (arrows in Fig. 1*K, J*), and autolysosomes (asterisks in Fig. 1*L*) in the motor neurons of the SALS patients, which were scarcely observed in the control patients.

### Generation of the *dnc-1*-depleted *C. elegans* model

To examine the relationship between the loss of dynactin 1, the accumulation of autophagosomes, and motor neuron degeneration, we created a *dnc-1*-KD *C. elegans* model by transfecting *C. elegans* with a plasmid expressing an shRNA and GFP under the control of the motor neuron-specific *acr2* promoter (*dnc-1(RNAi)*). In the transgenic worms, GFP was expressed diffusely in ventral motor neurons (Fig. 2*A*). We confirmed the effect of RNA interference on the level of endogenous *dnc-1* mRNA using whole mount *in situ* hybridization. In the *control(RNAi)* worms, *dnc-1* expression was not altered by *shRNA::GFP* expression (Fig. 2*B*). Conversely, in the *dnc-1(RNAi)* worms, motor neurons expressing *shRNA::GFP* exhibited reduced or no expression of *dnc-1* (Fig. 2*B*). As shown in Fig. 2*C*, approximately 22 neurons were GFP-positive both in the *control(RNAi)* and *dnc-1(RNAi)* worms. The number of *dnc-1*-positive motor neurons was decreased by approximately 20 (*control(RNAi)* worms, 35.3±3.8; *dnc-1(RNAi)* worms, 15.9±9.8), suggesting that *dnc-1* was successfully knocked down in almost all the GFP-positive cells (Fig. 2*C, D*). Moreover, *dnc-1* expression was not affected in the head sensory neurons of the *dnc-1(RNAi)* worms, confirming the specificity of the promoter (Fig. 2*E*). Taking these results into account, in the following experiments, we selected the *dnc-1(RNAi)* and *control(RNAi)* worms expressing GFP in more than 30 motor neurons to avoid the influence of knockdown efficiency on the experimental results.

### Motor dysfunction in motor neuron-specific *dnc-1*-KD *C. elegans*

The *dnc-1(RNAi)* worms demonstrated uncoordinated locomotion (Fig. 3*A*), which is a phenotype observed in *C. elegans* mutant models of motor neuronal defects [30,31]. Maturation of the worms resulted in the progressive aggravation of their uncoordinated locomotion, characterized by partial paralysis, slowed movement, and coiling. The feeding plate of the *dnc-1(RNAi)* worms appeared to be stagnated, as they only ate the food around themselves due to their decreased motility (Fig. 3*A*). As described in the Materials and Methods, we generated six lines of *dnc-1(RNAi)* worms: SBG7, 8, and 15 using shRNA1(101), and SBG20, 24, and 25 using shRNA2(2888). Survival analysis and body bend assays were performed using these six lines. Since these animals exhibited almost the same phenotype, SBG8 was employed for further analysis. Compared with the *control(RNAi)* worms, the *dnc-1(RNAi)* worms had a decreased life span (Fig. 3*B, C*) (11.4±4.4, 11.2±3.0, 13.4±4.0, and 14.3±3.3 days for *dnc-1(RNAi-1)*, *dnc-1(RNAi-2)*, *control(RNAi)*, and wild-type worms, respectively). *dnc-1(RNAi)* worms also exhibited significantly reduced bending and thrashing rates that declined with age
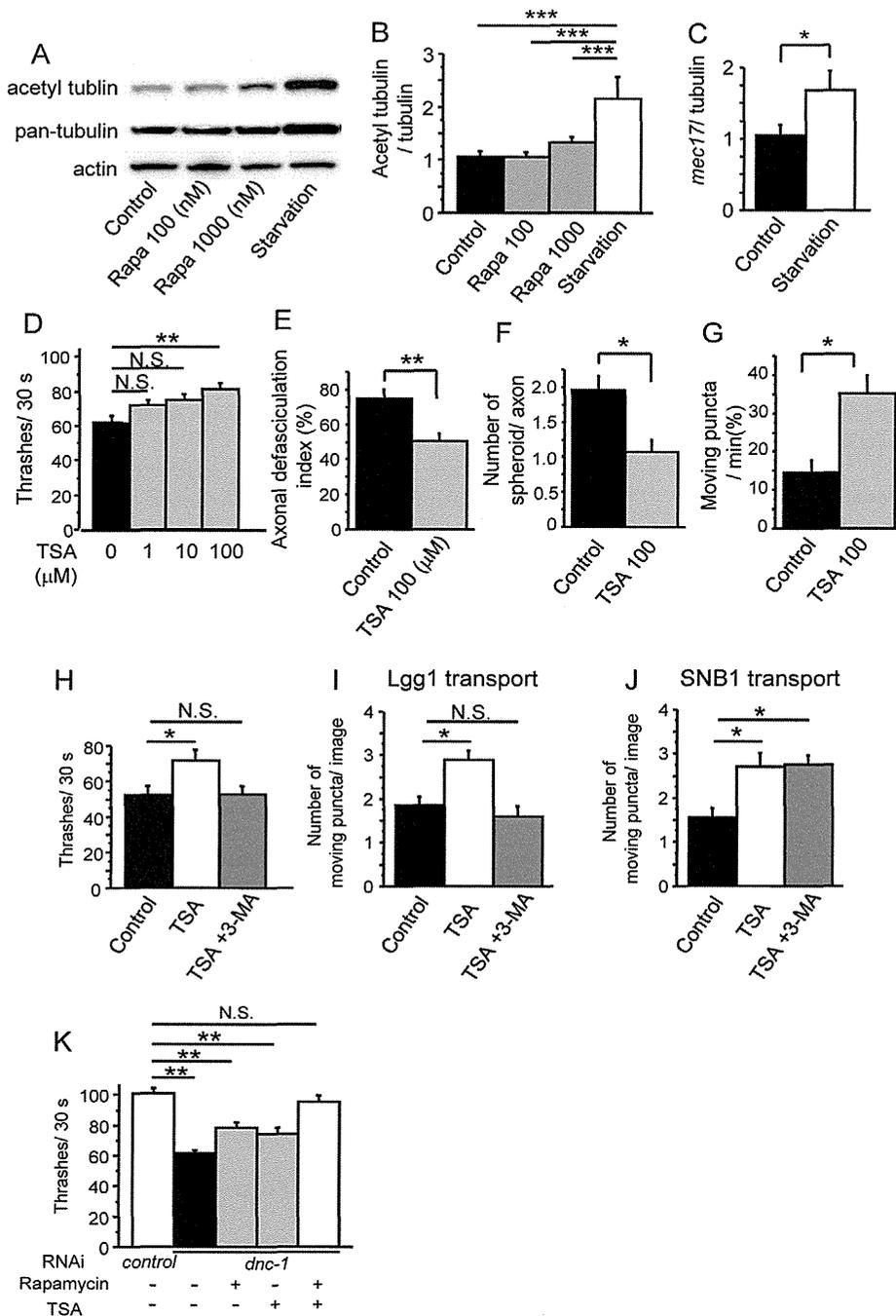
**Figure 11. The effects of tubulin acetylation on the transport of autophagosome and neurodegneration in the** *dnc-1(RNAi)* **worms.**
(*A, B*) Immunoblots of primary cultured cells using antibodies against acetylated tubulin, pan-tubulin, and actin (n = 5). (*C*) The mRNA levels of *mec17* measured by real-time RT-PCR. The data shown are ratios to the mRNA levels of *tba1*, the gene encoding alpha-tubulin. (*D*) Effect of trichostatin A (TSA) on the locomotor function of the *dnc-1(RNAi)* worms (n = 35 for each group). (*E–G*) Effect of TSA (100 μM) on the axonal degeneration of the *dnc-1(RNAi)* worms (*E, F*) and on autophagosome mobility (*G*) (n = 15 for each group). (*H*) The inhibition of autophagy by 3-MA (10 mM) negates the effect of TSA treatment on the motor function of the *dnc-1(RNAi)* worms (n = 35 for each group). (*I, J*) The number of moving puncta (*I*, Lgg1; *J*, SNB1) was counted using kymographs derived from *in vivo* time-lapse images (n = 20 images for each analysis). Treatment with 3-MA negates the effect of TSA treatment on the transport of Lgg1 (*I*), but not the transport of SNB1 (*J*). (*K*) Combination therapy of rapamycin (100 μM) and TSA (100 μM) has synergistic effects on the locomotive functions of the *dnc-1(RNAi)* worms (n = 35 for each group). Statistical analyses were performed by one-way ANOVA followed by the Bonferroni/Dunn post hoc test for (*B*), Dunnett's post hoc test (*D, H–K*), and Student's t test (*C, E–G*) ($*p < 0.05$, $**p < 0.001$, and $***p < 0.0001$). The error bars are S.E.M.
doi:10.1371/journal.pone.0054511.g011

(Fig. 3*D*, *E*). The thrashing speed of the *control(RNAi)* worms was slightly decreased compared with the wild-type worms, possibly due to the toxicity of GFP, as previously reported [32] (Fig. 3*E*).

Although the toxicity of GFP was much less than that of *dnc-1* knockdown and not detectable in the bending assay, to exclude any effects of the fluorescent protein on our analysis, we compared

- 134 -

the *dnc-1(RNAi)* worms with the *control(RNAi)* worms, both of which express GFP at similar levels, in all experiments. We also performed a video capture analysis to visualize the movement trace of each worm and measure its average speed (Fig. 3*F*, *G*). The movement speed was dramatically decreased in the *dnc-1(RNAi)* worms compared with the *control(RNAi)* worms at an early adult stage.

## Axonal degeneration is the early sign of neurodegeneration in the *dnc-1(RNAi)* worms

We then examined the morphological changes in the *dnc-1(RNAi)* worms using fluorescent microscopy. In normal worms, the ventral nerve cords were tightly fasciculated and the motor-neuron cell bodies (white asterisks in Fig. 4*A*) were round or ovoid. (Fig. 4*B*, *C*). By contrast, we found irregular shapes and defasciculation of the ventral nerve cord as well as axonal swellings, or spheroids, in the *dnc-1(RNAi)* worms at an early stage (Fig. 4*D*). At this early stage (4 days old), the cell bodies in the *dnc-1(RNAi)* worms seemed normal judging from their shape and structure (Fig. 4*D*). However, at a later adult stage (7 days old), axonal degeneration was exacerbated and morphological changes were also detected in the cell bodies (Fig. 4*E*). Axonal changes were occasionally observed in the *control(RNAi)* worms with aging, but they were less frequent and not as severe as in the *dnc-1(RNAi)* worms (Fig. 4*C*). Semi-quantification of the axonal and cell body changes showed that the axonal abnormalities were observed at day 4 and cell body deformation occurred at a later stage (Fig. 4*F*). Although some neurons exhibited an abnormal cell body shape at day 4, this change was only observed in the worms with axonal defasciculation (Fig. 4*G*), indicating that axonal degeneration occurs prior to cell body degeneration. Moreover, we also found that the severity of axonal defasciculation (i.e., the axonal defasciculation index) was correlated with locomotor dysfunction in the *dnc-1(RNAi)* worms (Fig. 4*H*). To clarify the time-course of the neuronal changes due to *dnc-1* depletion, we also examined the morphological change during the developmental stage. The acr2p::shRNA::GFP is not detectable before larval stage L1 (Fig. S1*A–C*). Furthermore, even after GFP is expressed, there was no alteration in morphology or motor phenotype during the larval stage (from L1 to L4, post natal days 1 and 2) (Fig. S1*C–E*). It was only after the worms became adult that the axonal degeneration and motor deficit appeared. Taken together, these findings suggest that the depletion of *dnc-1* induces the degeneration, rather than developmental defects, of motor neurons in *C. elegans*.

Further analysis via electron microscopy confirmed the axonal degeneration in the *dnc-1(RNAi)* worms (Fig. 5*C–F*). In the early degenerative stage, *dnc-1(RNAi)* worms first exhibited whorl like inclusions in axons with only a few morphological changes in their cell bodies (Fig. 5*C*, *D*) compared with *control(RNAi)* worms (Fig. 5*A*, *B*). In the later degenerative stage, strikingly abundant whorl-like inclusions and vacuoles, corresponding to degeneration and swelling of axons [21], were observed in axons and cell bodies (Fig. 5*E*, *F*).

## Axonal transport defect in the *dnc-1(RNAi)* worms

Abnormalities in the localization and accumulation of synaptic vesicles were reported in a *C. elegans* model showing a defect in axonal transport [20]. To determine whether our *dnc-1(RNAi)* model exhibited defects in axonal transport, we used a fluorescently tagged synaptic vesicle marker composed of the *C. elegans* VAMP2/synaptobrevin protein fused to DsRed (SNB-1::DsRed), and examined the distribution of the dorsally located red puncta (Fig. 6*A*). In the dorsal nerve cord (the axons of the ventral motor neurons) of the *control(RNAi)* worms, SNB-1::DsRed puncta were

regularly spaced, whereas the *dnc-1(RNAi)* worms exhibited a discontinuous and irregular distribution of the marker, including occasional clumps that may represent the accumulation of cargo proteins (Fig. 6*B*). Histograms of the distances between neighboring SNB-1 puncta displayed a broader curve in the *dnc-1(RNAi)* worms than in the *control(RNAi)* worms, suggesting some defect in axonal transport caused by the knockdown of *dnc-1* (Fig. 6*C*, *D*).

To demonstrate direct evidence of a defect in axonal transport in our transgenic worms, we monitored the movement of SNB-1 puncta by acquiring a series of time-lapse images. The resulting kymographs showed that puncta in the *dnc-1* KD worms were markedly static compared with those in the controls, confirming the disruption of axonal transport following the reduction of *dnc-1* in *C. elegans* (Fig. 6*E*, *F*, Movies S1, S2). To quantify the movement of SNB-1, we analyzed 20 kymographs from each strain. While there was no significant difference in the number of SNB-1 puncta between the *control(RNAi)* and *dnc-1(RNAi)* worms (Fig. 6*G*), the number of moving puncta (moving more than 2 μm) (Fig. 6*H*) and the ratio of moving puncta to total puncta (Fig. 6*I*) were significantly decreased in the *dnc-1(RNAi)* worms compared to the *control(RNAi)* worms (p = 0.028 and p = 0.014, respectively). The velocity of SNB-1 transport in the *dnc-1(RNAi)* worms was significantly lower than in the *control(RNAi)* worms (p<0.0001, Fig. 6*J*).

## Impaired transport and accumulation of autophagosomes in the *dnc-1(RNAi)* worms

We next investigated the effects of *dnc-1* depletion on autophagy in *C. elegans*. Autophagosomes are cargo that moves bidirectionally along microtubules, powered by the kinesin family of motor proteins and dynein/dynactin complexes [11,12]. Altered autophagy has been observed in several neurodegenerative models, including the mutant *DCTN1* mouse model [9,16,33,34]. However, little is known about the relationship between the decreased levels of dynactin 1 and the alteration of autophagy. To clarify the effect of quantitative loss of DNC-1/dynactin 1 in the transport of autophagosomes, we performed live-cell imaging analyses of autophagosome transport in the axons of primary cultured motor neurons from the *dnc-1(RNAi)* and *control(RNAi)* worms that co-expressed DsRed-tagged Lgg1/ATG8, which is associated with the autophagic membrane, in ventral motor neurons under the control of the *acr2* promoter (Mizushima et al. [35]. This marker of autophagosomes is expressed diffusely in the ventral motor neurons (Fig. S2*A*) and forms distinct puncta when autophagosomes are formed (Fig. S2*B*) [36]. In the *control(RNAi)* neurons, the fluorescent Lgg1 vesicles moved toward and away from the cell body, suggesting that these vesicles are powered by anterograde and retrograde motors (Fig. 7*A*, Movie S3). By contrast, in the *dnc-1(RNAi)* worms, the autophagosomes were easily trapped where the axon was tight or curved, or at spheroids (Fig. 7*B*, Movie S4). This phenomenon was followed by the accumulation of autophagosomes distal to the trapped sites. Histograms showing the distribution of the velocity and distance of autophagosome movement demonstrated a significant loss of fast- and long-moving vesicles in the *dnc-1(RNAi)* cells compared with the *control(RNAi)* cells (Fig. 7*C*, *D*). The mean velocity and movement distance (run-length) were significantly decreased in the antero-grade and retrograde directions in the *dnc-1(RNAi)* neurons (p<0.0001, = 0.0001; velocity of anterograde, retrograde movements, respectively, and p = 0.0045, <0.0001; run-length of anterograde, retrograde movements, respectively) (Fig. 7*E*, *F*).

Next, we performed kymograph analysis of Lgg1::DsRed using *in vivo* time-lapse images (Fig. 8*A*, *B*, Movie S5, S6). Although the total number of Lgg1 puncta was significantly increased

(p<0.0001) (Fig. 8C), the number (Fig. 8D) and the ratio of moving puncta (Fig. 8E) were significantly decreased in the *dnc-1(RNAi)* worms compared with the *control(RNAi)* worms (p = 0.013 and p<0.0001, respectively). The velocity of Lgg1 movement was also significantly decreased in the *dnc-1(RNAi)* worms (p<0.0001) (Fig. 8F). These results indicated that the *dnc-1* depletion resulted in the accumulation of untransported autophagosomes in the motor neurons.

We then investigated whether the accumulation of autophagosomes is related to the motor neuron degeneration. In the ventral nerve cord of the *dnc-1(RNAi)* worms, the number of Lgg1 puncta was significantly increased in comparison with the *control(RNAi)* worms (p = 0.019) (Fig. 8G), and the accumulation of autophagosomes was correlated with the axonal defasciculation index and locomotor function (Fig. 8H, I). We also explored the localization of Lgg1::DsRed in the distal ascending axon and observed Lgg1::DsRed accumulation in axonal spheroids (Fig. S2C), which is consistent with a previous report showing the abnormal accumulation of disorganized organelles and autophagosomes in axonal spheroids [37]. Electron microscopy showed that the accumulation of vesicular structures, including autophagosome-like vesicles and mitochondria, was observed in the proximal axons or cytoplasm of the *dnc-1(RNAi)* worms, although such accumulations were detected rarely in the axons of the *control(RNAi)* neurons (Fig. 8J–L).

We then treated the *control(RNAi)* worms with 3-MA, which inhibits the formation of autophagosomes (Fig. 9A). These worms showed the locomotory defects and axonal degeneration observed in the *dnc-1(RNAi)* worms, suggesting that the disrupted autophagy system is sufficient to cause the motor neuronal degeneration in this model (Fig. 9B–E). On the other hand, when we treated the *dnc-1(RNAi)* worms with 3-MA, worms did not exhibit a substantial change in the motor function or in the axonal integrity (Fig. 9F–H).

## Starvation dramatically attenuates the motor deficits in the *dnc-1(RNAi)* worms by facilitating the axonal transport of autophagosomes

Autophagy is known to be activated by rapamycin, a specific inhibitor of the mTOR pathway [38]. Starvation is also a strong activator of autophagy; however, it also has other effects, e.g., activation of the mitogen-activated protein kinase (MAPK) pathway [39], stimulation of tubulin acetylation [40], and induction of sirtuin [41]. Both treatments have been used widely in many species, e.g., *Drosophila*, mouse, and *C. elegans*, to activate autophagy [42–44].

To study the effects of autophagy activators on axonal degeneration in *C. elegans*, we treated the *control(RNAi)* and *dnc-1(RNAi)* worms with rapamycin or starved them by food restriction, and investigated the changes in motor function via the liquid thrashing assay. Rapamycin and starvation are known to extend lifespan of *C. elegans* [42,45]. In the present study, we found that neither rapamycin nor starvation significantly altered the motor function of the *control(RNAi)* worms (Fig. 10A). In the *dnc-1(RNAi)* worms, rapamycin ameliorated the thrashing activity in a dose-dependent manner, although it showed only a limited effect even at the most effective dose (Fig. 10A). In contrast, starvation completely ameliorated the motor dysfunction of the *dnc-1(RNAi)* worms without affecting the efficiency of *dnc-1* knockdown (Fig. 10A, Fig. S3A–C). The formation of axonal spheroids was also significantly suppressed by starvation (p = 0.001) (Fig. 10B, C). Given the differential effects of rapamycin and starvation, we hypothesized that starvation not only increases the formation of autophagosomes but also increases their mobility in axons. Indeed,

the frequency of autophagosome movement was increased by food restriction (Fig. 10D). To further confirm this hypothesis, we cultured primary motor neurons from the *dnc-1(RNAi)* worms in serum-depleted medium, and quantified the mobility of autophagosomes by monitoring the movement of DsRed-tagged Lgg1 in axons. As we expected, starvation significantly increased the speed and run-length of moving Lgg1 puncta, especially the retrograde run-length, in the *dnc-1(RNAi)* worms (p<0.0001) (Fig. 10E, F). Conversely, neurons treated with rapamycin showed no detectable change in the transport of autophagosomes (Fig. 10E, F). Histograms showing the distribution of the velocity and distance of autophagosome movement also demonstrated a significant increase of fast- and long-moving vesicles in the starved cells, especially in retrograde transport (Fig. 10G, H). For example, the percentage of vesicles that moved more than 8 μm retrogradely increased from 6.9% (*dnc-1(RNAi)* control) to 27.0% (*dnc-1(RNAi)* starvation), whereas the change was only from 12.7% to 19.7% in the anterograde direction (Fig. 10H).

Finally, we investigated how starvation stimulates the axonal transport of autophagosomes and assessed whether drugs that mimic the molecular mechanisms of starvation enhanced its effect. The acetylation of tubulin is known to stabilize microtubules and activate axonal transport by the subsequent recruitment of the molecular motors kinesin-1 and dynein/dynactin to microtubules [46,47]. Therefore, we assessed the acetylation state of alpha-tubulin in our cultured cell assay. Starvation increased the levels of acetylated tubulin, but this effect was not detected in cells treated with rapamycin (Fig. 11A, B). Moreover, real-time quantitative PCR demonstrated that starvation, but not rapamycin, significantly increased the mRNA levels of *mec-17*, an enzyme that acetylates tubulin in *C. elegans* [48] (Fig. 11C). Taken together, our results suggest the possibility that starvation mitigated axonal degeneration by activating autophagy and promoting the axonal transport of autophagosomes via the acetylation of tubulin in the *dnc-1(RNAi)* worms. To test this hypothesis, we examined the effects of TSA, an HDAC inhibitor that facilitates tubulin acetylation, on the phenotypes of the *dnc-1(RNAi)* worms. Although treatment with TSA did not exhibit substantial effects on the phenotype of the *control(RNAi)* worms (Fig. S4A–C), this treatment showed a significant effect on the locomotory function of the *dnc-1(RNAi)* worms in a dose-dependent manner, and attenuated the axonal degeneration without alteration of *dnc-1* knockdown efficiency (Fig. 11D–F, Fig. S3A, B, and D). As expected, TSA increased the mobility of autophagosomes (Fig. 11G). Interestingly, treatment with 3-MA dampened the effect of TSA on locomotion (Fig. 11H). On the contrary, the worms treated with both TSA and 3-MA showed decreased transport of autophagosomes without defects in the transport of synaptobrevin (Fig. 11I, J). Furthermore, we also examined the effect of combination therapy with rapamycin and TSA. Although treatment with rapamycin or TSA alone had limited effects in comparison with *control(RNAi)* worms, the combination of rapamycin and TSA had greater effects such that locomotion was restored in the worms treated with these two drugs to the levels observed in the *control(RNAi)* worms (Fig. 11K).

## Discussion

In the present study, we generated a novel *C. elegans* model that mimics the down-regulation of dynactin 1 observed in the motor neurons of SALS patients. Using this model, we investigated whether the quantitative loss of DNC-1/dynactin 1 causes motor neuron degeneration. Our results showed that the knockdown of *dnc-1* caused progressive motor deficits in *C. elegans*, and the

- 136 -